MODELING OF SURGE AND SWAB PRESSURE OF YIELD POWER LAW FLUIDS

A THESIS SUBMITTED TO
THE GRADUATE SCHOOL OF NATURAL AND APPLIED SCIENCES
OF
MIDDLE EAST TECHNICAL UNIVERSITY

BY

ÖNER ERGE

IN PARTIAL FULFILLMENT OF THE REQUIREMENTS
FOR
THE DEGREE OF MASTER OF SCIENCE
IN
PETROLEUM AND NATURAL GAS ENGINEERING

SEPTEMBER 2016

Approval of the Thesis:

MODELING OF SURGE AND SWAB PRESSURE OF YIELD POWER LAW FLUIDS

submitted by **ÖNER ERGE** in partial fulfillment of the requirements for the degree of **Master of Science in Petroleum and Natural Gas Engineering Department, Middle East Technical University** by,

Prof. Dr. Gülbin Dural Ünver
Dean, Graduate School of **Natural and Applied Sciences** _____

Prof. Dr. Serhat Akın
Head of Department, **Petroleum and Natural Gas Engineering** _____

Prof. Dr. Serhat Akın
Supervisor, **Petroleum and Natural Gas Engineering Dept., METU** _____

Assoc. Prof. Dr. İsmail Hakkı Gücüyener
Co-supervisor, **GEOS Energy Inc.** _____

Examining Committee Members:

Prof. Dr. Mahmut Parlaktuna
Petroleum and Natural Gas Engineering Dept., METU _____

Prof. Dr. Serhat Akın
Petroleum and Natural Gas Engineering Dept., METU _____

Assoc. Prof. Dr. İsmail Hakkı Gücüyener
GEOS Energy Inc. _____

Asst. Prof. Çağlar Sınayuç
Petroleum and Natural Gas Engineering Dept., METU _____

Asst. Prof. Tuna Eren
Petroleum and Natural Gas Engineering Dept., Batman University _____

Date: 02.09.2016

I hereby declare that all information in this document has been obtained and presented in accordance with academic rules and ethical conduct. I also declare that, as required by these rules and conduct, I have fully cited and referenced all material and results that are not original to this work.

Name, Last name: Öner Erge
Signature:

ABSTRACT

MODELING OF SURGE AND SWAB PRESSURE OF YIELD POWER LAW FLUIDS

Erge, Öner

M.S., Department of Petroleum and Natural Gas Engineering

Supervisor: Prof. Dr. Serhat Akın

Co-supervisor: Assoc. Prof. Dr. İsmail Hakkı Gücüyener

September 2016, 84 pages

A mathematical modeling work and computational fluid dynamics (CFD) analysis of surge and swab pressures in concentric annuli is conducted. A commercial CFD package is used to validate the developed model of the flow during surge and swab in concentric annuli. Developed mathematical model incorporates the Yield Power Law (YPL) fluid behavior for closed-end pipes under laminar flow conditions. The results of the mathematical model and CFD analysis is compared with the models from literature.

CFD analysis is initially compared with the analytical solution of the surge and swab velocity profiles of a Newtonian fluid to validate the CFD approach. A good agreement is obtained with the analytical solution and the results from the CFD analysis. A similar approach is followed and proposed numerical solution is compared with the results from the CFD analysis to validate the proposed approach. A good agreement is observed with the result from CFD and the proposed finite differencing scheme. Velocity profile comparison among numerical solution, analytical solution and CFD analysis yields less than 5% average absolute percent error. A 3D geometry of concentric annuli is used in the CFD analysis. Also, a mathematical model is developed considering an annular geometry

with different inner and outer pipe sizes. The effect of the degree of curvature difference between the inner and outer pipes while surge and swab is captured both with the CFD analysis and the mathematical model. With this approach, more accurate results are obtained than approximating the annuli to a slot. Additionally, dimensionless velocity profiles are presented that better explain the flow during surge and swab conditions in concentric annuli while the inner pipe is reciprocating in steady-state.

Most of the drilling fluids can be characterized with Yield Power Law (YPL) model. YPL model includes a yield stress term similar to Bingham Plastic and has the shear thinning ability as the Power Law fluids. YPL model accurately estimates the drilling fluid behavior in low and high shear rates. After drilling, pulling out or running a BHA in the vertical section or running casing with centralizers approximates the position of the tubular to concentric. Therefore, mathematical modeling and CFD analysis of the swab and surge pressures of YPL fluids in concentric annuli has potential to optimize the tripping operations that will help not only avoid hole problems, but also reduce the non-productive time.

Keywords: Surge and swab pressure, yield power law, CFD, numerical modeling

ÖZ

YIELD POWER LAW AKIŞKAN İÇİN SURGE VE SWAB BASINCI MODELLEMESİ

Erge, Öner
Yüksek Lisans, Petrol ve Doğal Gaz Mühendisliği Bölümü
Tez Yöneticisi: Prof. Dr. Serhat Akın
Eş Tez Yöneticisi: Doç. Dr. İsmail Hakkı Gücüyener

Eylül 2016, 84 sayfa

Bu tezde, surge ve swab basınçlarının eş merkezli anülüste matematiksel model çözümlemesi ve hesaplamalı akışkanlar dinamiği analizi yapildi. Surge ve swab sırasında oluşan akış için oluşturulan matematiksel model, ticari bir hesaplamalı akışkanlar dinamiği programı ile kontrol edildi ve doğrulandı. Matematiksel model, kapalı uçlu sondaj dizisi ile surge ve swab sırasında oluşan laminer akış için Yield Power Law akış modeli uygulanarak çözüldü.

Hesaplamalı akışkanlar dinamiği analizinin doğruluğunu kontrol etmek için, sonuçlar ilk önce Newtonian akışkanın surge ve swab sırasında anülüste oluşan hız profilinin analitik çözümü ile karşılaştırıldı. Analitik çözüm ve hesaplamalı akışkanlar dinamiği sonuçları birbiriyle çok iyi oranda örtüştü. Aynı yaklaşım nümerik çözümü doğrulamak için de kullanıldı. Sonlu farklar yöntemi ile oluşturulan nümerik çözüm ve hesaplamalı akışkanlar dinamiği analizi sonuçlarının çok iyi oranda örtüştüğü görüldü. Anülüste oluşan hız profili sonuçları karşılaştırıldığında ortalama mutlak hata yüzdesinin %5'in altında olduğu görüldü. Hesaplamalı akışkanlar dinamiği analizinde eşmerkezli anülüsün 3 boyutlu

geometrisi kullanıldı. Ayrıca, matematiksel model, farklı iç ve dış çapları olan borular içeren bir anüler geometri düşünülerek hazırlandı. Böylece, hem hesaplamalı akışkanlar dinamiği analizi, hem de nümerik çözüm, iç ve dış borular arasındakı kıvrım derecesi farkının etkisini kapsamış oldu. Bu yaklaşım ile problemin anülüsü dar oluk benzetimi ile çözülmesinden daha doğru bir sonuç elde edildi. Analiz sonuçları boyutsuz hız profili grafikleri ile sunuldu; böylece eşmerkezli anülüste iç borunun yukarı aşağı kararlı durumdaki hareketi daha iyi bir şekilde anlaşıldı.

Çoğu sondaj akışkanının akış modeli Yield Power Law ile karakterize edilebilir. YPL modeli Bingham Plastic modelindekine benzer bir kopma gerilimi terimi, ve Power Law modelindeki gibi kayma incelmesi özelliğini içeren bir akış modelidir. YPL modeli, sondaj akışkanlarının hem düşük hem de yüksek kayma hızlarındaki davranışını doğru bir şekilde tanımlar.

Dikey sondajlarda, sondaj sonrasında sondaj dizisini kuyudan çıkarmak veya yeni bir dizi ile inmek, veya koruma borularını merkezleyici ile birlikte indirmek, kuyu içindeki boruların kuyu ile eşmerkezli olmasını yakınsar. Bu yüzden, YPL sondaj akışkanları kullanılarak yapılan eşmerkezli anülüsteki surge ve swab basınçlarının matematiksel model ve hesaplamalı akışkanlar dinamiği analizi sonuçları, iniş/çıkış manevralarını optimize etme potansiyeline sahiptir. Böylece, hem kuyu problemlerinin önüne geçilmiş olur, hem de sondaj operasyonlarındaki kayıp zaman azalır.

Anahtar Kelimeler: Surge ve swab basıncı, yield power law, hesaplamalı akışkanlar dinamiği, nümerik model

to my beloved family…

ACKNOWLEDGEMENTS

First of all, I would like to express my deepest gratitude to my supervisor Prof. Dr. Serhat Akın for his encourage, patience, advices, and support. Without his guidance and valuable advices, this work would be incomplete.

I wish to thank to my co-advisor Assoc. Prof. Dr. İsmail Hakkı Gücüyener. His knowledge and work discipline inspired me immeasurably. Also, his insightful comments helped this work reach its current quality.

Sincere appreciations also deserved by a fellow friend of mine, Gökay Canal, who helped me both technically and morally throughout the research.

I would like to express my deepest thanks to my beloved family Nursel Erge, Bahattin Erge, and Selin Güven for their endless support. It is a privilege to have you. Special gratitude belongs to my brother, Öney Erge, for his patient struggle to help improving my technical knowledge.

This thesis is dedicated to my family.

NOMENCLATURE

K	Consistency Index, $Pa.s^n$
n	Flow Behavior Index
P	Pressure, Pa
L	Length, m
r	Radius, m
R_i	Inner Radius, m
R_o	Outer Radius, m
R_d	Dimensionless Radius
V_z	Velocity in z-direction, m/s
V_d	Dimensionless Velocity
V_p	Pipe Velocity, m/s
V_∞	Pipe Velocity, m/s
P_z	Pressure Gradient, Pa/m
ρ	Density, kg/m^3
μ	Viscosity, kg/m-s
τ	Shear Stress, Pa
τ_y	Yield Stress, Pa
γ	Shear Rate, s^{-1}
μ_p	Plastic Viscosity, Pa.s
λ	Geometric Constant Where Momentum Flux is Zero
κ	Dilatational Viscosity
$\nabla \cdot V$	Divergence of Velocity Vector

TABLE OF CONTENTS

LIST OF FIGURES

FIGURES

LIST OF TABLES

TABLES

CHAPTER 1

INTRODUCTION

During drilling, the drillstring can be moved out or moved into the wellbore for various reasons such as changing the BHA, changing the bit, etc. The drillstring will be disassembled or reassembled by making up or breaking out the tubulars that composes the drillstring and will be run in hole or pulled out of hole. This ascend and descend of the drillstring to a certain position is referred to as the tripping operation.

Tripping operations can be significantly costly due to long duration and possible hazards that may occur during running in or pulling out the drillstring. If swab and surge pressure is not well understood, reciprocation of the drillstring can easily cause a well integrity problem and/or a well control issue. During tripping out, crossing the collapse gradient can result in excessive cavings that can pack off around the stabilizers and bit, and can cause a well stability problem. Excessive speed during tripping out can swab the well, resulting an influx from the formation to the wellbore, especially at deep wells with a narrow operating margin between the pore and fracture pressure. Surge while running in bottomhole assembly (BHA) can increase the equivalent circulating density (ECD) over the fracture gradient that will induce a fracture and it would be followed by the fluid loss to the formation. Especially while running casing, significant surges occur and can lead to loss circulation, which will be followed by unsuccessful cementing operation and consequently poor zonal isolation, may be the loss of the hole. These issues can potentially be avoided, if the pressure changes due to the axial motion of the drillstring are better understood and managed.

A representative fluid model of the actual drilling operation should be used to understand the surge and swab pressure accurately. Yield Power Law model should be used to capture the low and high shear behavior of today's most common drilling fluids. In common practice, a check-valve is placed inside the drillstring to avoid annular fluid coming inside the drillstring. A mud motor also can act as a check valve that does not let fluid back inside the drillstring. Also during casing operations, a float collar and a float shoe might be part of the casing string that does not let fluid inside the tubular. Therefore, in most of the cases a closed end pipe can be present at drilling operations. When the drillstring is moved out, the annular fluid moves to the bottom to replace the volume of the tubular and the volume of the fluid inside the tubular. When the drillstring is moved in the annular fluid will be displaced the the volume of the tubular and the volume of the fluid inside the tubular.

Moving the drillstring in or out from the static condition will change the equivalent static density (ESD) to the equivalent circulating density (ECD). ECD can be lower than ESD if the drillstring is moved out, which is referred as swab pressure and can be higher while the drillstring being moved in, which is referred as surge pressure.

Swab and surge pressures can be very significant and can move ECD outside of the safe "mud" window, which is the interval between pore and fracture pressures of the wellbore. During tripping out swab pressure can move ECD below the collapse or pore pressure that will create hole problems or a well control situation due to an influx of formation fluid into the wellbore. While tripping in, surge pressure can move ECD to be higher than the fracture pressure that will fracture the formation and lost circulation will happen. To avoid these adverse conditions, surge and swab pressures of the wellbore considering the geometry, fluid properties, etc. should be well understood so that the operation can commence within the safe mud window and the tripping speed can be optimized to reduce overall time of the well construction process.

CHAPTER 2

LITERATURE REVIEW

Pressure changes in the well due to axial movement of tubular were investigated throughout the history of drilling. It was Cannon (1934), to make the first research on the swabbing effect. The study was based on investigation of effects of viscosity, gel strength and density of the drilling fluid, effects of depth, tripping speed, annular clearance, and bottom of assembly being open-ended or closed-ended on the pressure change due to withdrawal of drillpipe from the hole. However, lack of number of runs, insufficient equipment and unsuitable conditions made it hard to establish solid relationships among which drilling parameters to affect the pressure changes most.

Goins et al. (1951) investigated parameters affecting surge pressure. It is stated that increase in pressure due to running drilling assembly into hole is proportional with the depth. As the depth increases the surge pressure increases. They also noted that slow breaking of circulation and reducing tripping speed reduces the surge pressure. This suggest that the speed and the acceleration of the drillstring are the actuators to be controlled to manage the surge pressure.

Cardwell (1934) tried to explain the origin and magnitude of swab and surge pressures considering effects of viscosity and annular geometry. He was the first to publish a quantitative theory for pressure variations in the well due to swab and surge of Newtonian fluid during laminar flow. Despite the fact that drilling fluids are mostly far away from Newtonian nature, in some cases his results were reasonably accurate for maximum surge pressures, and practical, since they were presented in a convenient way for field use.

Ormsby (1954) formulated linear average annular velocities of drilling fluids for pulling out and running in drilling assembly. He took into account the cases of the bottom of tubular being closed-ended, partially open-ended and fully open-ended. Pressure drop and critical velocity equations for both laminar and turbulent flow of Bingham Plastic fluids were taken from Beck et al. (1947) and converted into field units. Approximate lower critical velocity was obtained using hydraulic diameter and flow properties of drilling fluids, which were determined by multispeed viscometers. By comparing the lower critical velocity and average annular velocity; flow regime, and eventually pressure drop was calculated and presented.

Clark (1955) studied surge pressure in concentric annuli for Bingham Plastic fluids. He presented equations of annulus flow velocities as a function of pipe velocity for both laminar and turbulent flows. Also, lower critical velocity values for transition from laminar to turbulent flow were formulated. In addition to pressure changes due to viscous drag of drilling fluids, inertial effects were also considered. General equations for Reynolds number for turbulent flow and necessary friction factor approximation graphs were presented. He provided surge and swab pressure drop equations with sample scenarios with related figures.

Burkhardt (1961) published a paper, which supplemented previous researches conducted by (Cannon, 1934, Goins et al., 1951, Cardwell, 1953, and Ormsby, 1954). He provided theoretical description of pressure surges and reported that the velocity profile in the annulus due to surge would depend on fluid viscous model (either Bingham plastic or Newtonian), annular geometry, flow type (either laminar or turbulent), and tripping speed. Then he analyzed each parameter for both closed-ended and open-ended bottom for how they affect the viscous drag related surge pressure. He presented equations for annular velocity, pressure drop and relevant equations of Bingham plastic fluids for both laminar and turbulent flows.

Schuh (1964) presented an approximate numerical model of surge and swab pressures for Power Law fluids in concentric annuli. The model accounted for both laminar and

turbulent flow of fluid caused by axial motion of inner pipe. He implemented the model into a computer program, input of which consisted of plastic viscosity, yield point, gel strength and density of drilling fluid, tripping speed, and annular geometry. The program provided the output of bottom hole pressure generated by surge.

Flumerfelt et al. (1969) studied generalized Couette Flow, which is defined as flow between two parallel surfaces, one of which is moving whereas the other is stationary. He presented dimensionless velocity profiles, volumetric flow rate and force on the fluid boundary equations with necessary tables and graphs. The analysis was conducted with laminar flow of Power law fluids.

Fontenot & Clark (1974) presented a comprehensive and general approach, including both Power Law and Bingham Plastic fluids, to calculate bottom hole pressure when surge and swab took place. They improved equations proposed by (Burkhardt, 1961 and Schuh, 1964) and implemented into a computer program. The program results were in accord with field measurements. This comparison revealed the importance of drilling fluid properties and annular velocity among the parameters that have impact on surge and swab pressures.

All of the analyses in the past studies regarding surge and swab pressure were time independent, and most of them were based on surge or swab with laminar flow of either Newtonian or Bingham Plastic fluid in concentric annulus.

Lubinski et al. (1977) was the first to develop fully dynamic unsteady-state model for swab and surge pressure. He modeled the drillstring transient motion and the swab/surge pressure that occur due to reciprocation of the drillstring.

Lin & Hsu (1980) presented a numerical solution for velocity distribution of generalized Couette flow of a Power law fluid in concentric annuli. MacSporran (1982) identified few deficiencies about the study of Lin and Hsu regarding the velocity profile expressions. Shortly after, same authors corrected their studies in (Lin and Hsu, 1982).

Lal (1983) presented a dynamic surge and swab model and a computer program, which employed Power Law fluids. The program predicted maximum surge pressure with its time variation, and maximum safe tripping speed. To understand the effects of various parameters on surge and swab pressure, a sensitivity analysis was conducted for various wells. The input parameters included tripping depth, annular geometry, drilling fluid properties, and tripping speed. He listed the parameters affecting swab and surge pressures by assigning their importance. He also compared his unsteady-state model results with the steady-state model results of Burkhardt (1961), and presented the differences.

Mitchell (1988) developed a dynamic surge model for laminar flow of Power Law fluid. Apart from being on transient model, the novelty of his model was the inclusion of pressure and temperature dependent drilling fluid properties (i.e plastic viscosity and yield point), pipe eccentricity and compressibility of the drilling fluid. He emphasized the effect of fluid compressibility on surge pressure becoming more pronounced in deep wells. He compared the model with the field data acquired form Burkhardt (1961), and Fontenot and Clark (1974). He stated that the dynamic surge model captured the pressure peaks during surge and it was in a better agreement with field data compared to steady-state models.

Malik & Shenoy (1991) investigated the steady-state laminar Couette flow of Power law fluids in concentric annuli. In addition to the work of Lin and Hsu (1980), Malik and Shenoy (1991) considered the pressure gradient being against the drag direction, i.e upward motion of moving cylinder. They derived and used a new generalized volumetric flow rate equation, which no longer requires definite integrals to solve.

Another non-Newtonian rheological model, Robertson-Stiff was investigated by Haige and Xisheng (1996) in the scope of steady surge and swab pressures in concentric annuli. They presented a theoretical model calculating surge and swab pressures caused by viscous drag of drilling fluids. The model incorporated the inclination of the wellbore, therefore applicable for directional wells. They formulated the annular velocity profile, volumetric flow rate and surge pressure using Robertson-Stiff rheological model with

several assumptions such as laminar steady state flow only. They reported a sample scenario to calculate the surge pressure in a directional well.

Bing et al. (1995) studied the steady-state surge and swab pressures of laminar flow of Herschel-Bulkley fluid in concentric annuli. He listed some shortcomings of previous dynamic models such as Lubinski et al. (1977), Lal (1983), and Mitchell (1988) being too complex for field use, and steady-state models apply only to the concentric annuli, etc. He proposed a model and presented velocity distribution, volumetric flow rate, and corresponding surge and swab pressures caused by clinging power during tripping with Herschel-Bulkley fluids. He also presented accompanying figures and an example for calculation of surge pressure in a sample well scenario.

Yang and Chukwu (1995) analyzed steady-state, laminar flow of Power law fluids in eccentric annuli to determine the surge and swab pressures during axial movement of drilling assembly. Analytical solution of equation of motion was reported and the solution was given in dimensionless parameters for general use. The family of curves for varying eccentricity ratios and flow behavior indices, and resulting dimensionless pressure gradients were shown. Using the dimensionless pressure gradients, one can practically estimate surge or swab pressure. They presented a case scenario to predict surge pressure for different eccentricity ratios. They also compared the surge pressure gradient generated from eccentric annuli and concentric annuli. It was found out that in concentric annuli, surge pressure gradient is greater than that of eccentric annuli.

Wang and Chukwu (1996) studied transient modeling of laminar Couette flow of Power law fluids in concentric annuli. They solved the equation of motion analytically by perturbation method. The resulting pressure gradient equations were presented in dimensionless forms for varying annular geometries and flow behavior indices of Power law model. They also generated family of curves from which the dimensionless pressure gradient was obtained. The authors stated that minimizing pipe acceleration was of great importance to help maintain formation stability.

Hussain and Sharif (1997) developed a numerical solution for surge and swab pressures caused by axial laminar flow of Herschel-Bulkley fluids in eccentric annuli during tripping. They considered partially blocked and fully open annuli in their study. A computer code involving finite difference scheme was developed, which accounted for an exponential model of shear stress. The numerical model covered the effects of generalized Bingham number, flow behavior index, eccentricity and cutting blockage height on generated surge pressure. The authors validated their model with analytical solution in a concentric annuli, since neither the analytical solution, nor the field or experimental data for eccentric annuli were available. They discovered that the pressure gradient from axial motion of inner pipe decreased with increasing eccentricity. Furthermore, their results showed that annuli with partial cutting blockage would generate lower surge pressure than the one without any blockage. It was reported that the surge pressure was inversely proportional with blockage height.

Samuel et al. (2003) compared real-time drilling data, obtained by measuring while drilling (MWD) tools during tripping and circulating, with a dynamic surge and swab model. The dynamic model developed by Mitchell (1988), which accounts for the effects of fluid inertia, compressibility, elasticity of wellbore and pipe, temperature-dependent drilling fluid properties, well deviation and eccentricity is used. The authors provided a total of 5 case studies from two different wells. The cases include swab, surge, reciprocating with and without circulation, and surge with circulation and rotation. Various different drilling fluids, annular geometries and tripping speeds were presented. Their results showed good agreement between the model and actual field data. They concluded that the dynamic surge and swab model was capable of accurately predicting the surge and swab pressures for a range of drilling parameters.

In a later study, Samuel (2010), emphasized the influence of coefficient of friction while calculating the transient surge and swab pressures. In the study, he analytically showed the importance of friction between the drillstring and the wellbore in several drilling operations considering the surge and swab pressures. He showed that even minor changes

in friction factor may cause significant underestimation or overestimation of surge and swab pressures, especially in highly deviated and extended reach wells.

Rommetveit et al. (2005) developed a dynamic surge and swab model that is able to simulate pressure and temperature at any point in wellbore. The authors validated their model with data obtained from an offshore well field study. They tested a set of drilling parameters, such as thermohydraulic effects between pressure and temperature, injection and monitoring of nitrogen migration in the riser, gel breaking pressures, and surge and swab pressures. Comparison between test results and the model showed that the simulation can reproduce the surge and swab pressures accurately, in the presence of acceleration effects.

Wolski et al. (2014) proposed an approach to predict surge and swab pressures for steady-state flow for upper ends of drill pipes and annuli being open to atmosphere. They assumed one-dimensional, fully developed and laminar flow of incompressible fluid. The pressure was caused by the axial movement of inner pipe in concentric annuli. They disregarded the effects of transient changes, geometric variations in drill pipes and annuli, and flow through nozzles. These assumptions were justified by suggesting that pressure losses due to transient motion, geometric variations and flow through nozzles are relatively small. The authors formulated shear rate and shear stress equations for Bingham Plastic fluid and provided dimensionless pressure gradient equation. They compared the results of the model with the experiments conducted with a Newtonian fluid. The experiments were conducted for a set of different annular geometries, and tripping speeds. Moreover, they compared the model with the approach proposed by Fontenot and Clark (1974). The results of comparison between previous and current model revealed that differences in pressure drop values were within an error range of 0 to 10%.

Rubiandini R.S. (2000) improved the model developed by Burkhardt (1961). He converted the velocity of pipe term into effective average mud velocity. Maximum mud velocity term was taken from Moore (1986).Consequently, he developed a formula for optimum safe tripping speeds without crossing the operating pressure window. The formula

accounted for mud properties (i.e plastic viscosity, yield point, mud weight), tripping speed, and annular geometry. He assumed closed-ended pipe at bottom, and steady state flow of Bingham Plastic fluids in concentric annuli. The model was applicable to both laminar and turbulent flows. The author also validated his model with the field data presented in Burkhardt (1961). The comparison of resulting surge pressures between his model and field data was demonstrated by graphs.

Wagner et al. (1993) presented a comparison of surge and swab field data with a dynamic model for Power Law fluids, developed by Mitchell (1988). In addition to transient models of Lubinski et al. (1977) and Lal (1983), Mitchell's model considered the axial pipe elasticity and wellbore elasticity. Therefore, the dynamic model considered fluid inertia, fluid compressibility, wellbore and axial pipe elasticity, temperature dependent drilling fluid rheology and well deviation. Field tests were conducted for two different wells, one of which was an offshore well. The comparison between field data and model showed good agreement.

Crespo & Ahmed (2013) modeled steady-state laminar flow analysis of surge and swab of Yield Power Law fluids in concentric annuli using narrow-slot approximation. They also conducted experiments where the effects of drilling fluid properties, tripping speed and annular geometry on surge and swab pressures were investigated. A laboratory study was carried out using both Newtonian and non-Newtonian fluids. To validate their model, they compared the results with experimental data and existing models presented in the literature by Bourgoyne et al. (1991), Schuh (1964). They provided comparison graphs including family of curves for each affecting parameter. They stated that the changes in tripping speed, diameter ratio and yield stress of drilling fluid would have a proportional effect on surge and swab pressures. They concluded that an increase in the pipe eccentricity would reduce surge and swab pressures significantly. The results showed that the authors' correlation is in accord with experimental study and existing models.

2.1 Surge and Swab Pressure of Yield Power Law Fluids in Concentric Annuli

When the tubular is moved up or down, it excites the flow around the wall, as well as the fluid moves down, or up, to account for the tubular displacement. For example, while the closed end drillstring is moving down, annular fluid is displaced to move up in the annuli. At the same time, the fluid near the wall of the tubular, in the annuli, moves down with the drillstring.

When the drillstring is moving up, fluid in the annulus moves down to fill the volume of the displaced tubular at the bottom of the drillstring. At the same time, the fluid near and around the drillstring moves up.

These described scenarios can cause significant pressure losses in the annuli (or equivalent circulating density). Also, these scenarios can cause a velocity profile of multiple regions. A schematic drawing is described in Figure 2-1.

As it is presented in the Figure 2-1, three distinct regions can exist. They can be defined as:

- Region 1: Inner shear region, which is from the inner pipe to the plug region.
- Region 2: Plug region.
- Region 3: Outer shear region, which is from the end of the plug region to the outer wall/wellbore.

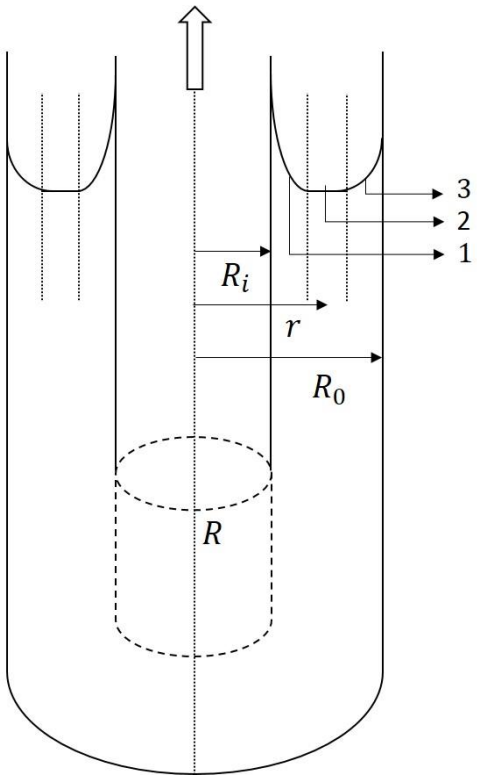

Figure 2-1. Laminar Velocity Profile in Annulus while Swabbing

2.2 Rheological Models

In general, fluids can be divided into two groups, based on their flow behavior: Newtonian fluids and non-Newtonian fluids.

An example shear stress versus shear rate figure of several rheological models is presented below in Figure 2-2:

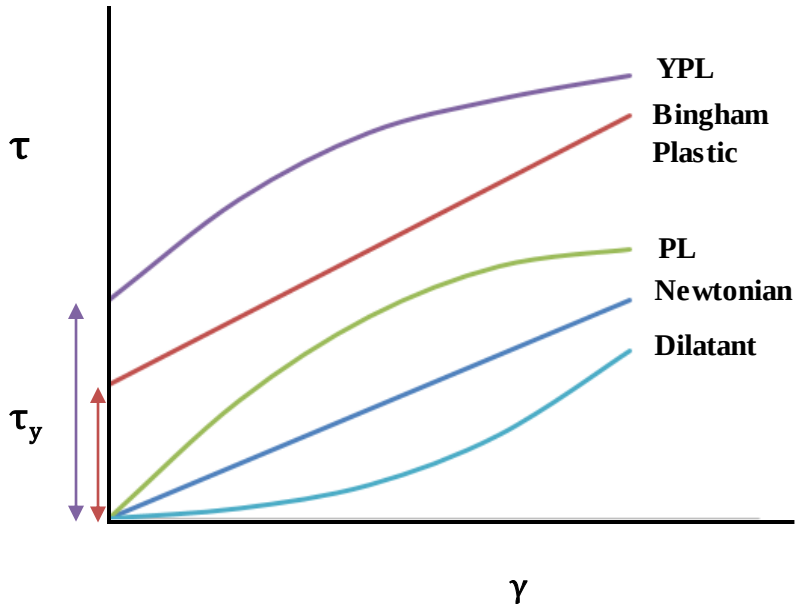

Figure 2-2. Rheological Models

Rheological models exemplified in the figure are further explained in this section.

2.2.1 Newtonian Fluids

Newtonian fluids exhibit direct proportionality between applied shear rate and shear stress (White, 2010). The ratio of shear stress to shear rate is defined as apparent viscosity. In this case, the apparent viscosity is constant and called as dynamic viscosity. Therefore, the shear stress equation for Newtonian fluids become:

$$\tau = \mu\gamma \tag{2-1}$$

2.2.2 Non-Newtonian Fluids

The fluids that cannot be described by a single value for viscosity, i.e, polymeric liquids, slurries, and some complex liquids and suspensions, are referred to as Non-Newtonian fluids (Bird et al., 2002).

Non-Newtonian fluids are divided into two subclasses; namely, shear thinning and shear-thickening fluids. Shear thinning fluids display a decrease in apparent viscosity with increasing shear rate. Non-Newtonian fluids are called shear-thickening (dilatant), if an increase in shear rate results in an increase in apparent viscosity.

Non-Newtonian fluid models are explained further in the following section:

2.2.2.1 Bingham Plastic

The Bingham Plastic model requires two parameters to characterize the flow: τ_y is yield point, representing the stress in order to initialize the flow; μ_p is plastic viscosity, denoting the constant of proportionality between shear stress and shear rate, after certain yield stress. Model is defined by:

$$\tau = \tau_y + \mu_p \gamma \tag{2-2}$$

In the case of zero threshold force for flow initiation i.e. $\tau_y = 0$, the model becomes equivalent to Newtonian model.

2.2.2.2 Power Law

The power law model is defined by:

$$\tau = K\gamma^n \tag{2-3}$$

Power law model has two parameters: K is consistency index, and n is flow behavior index. The deviation of flow behavior index from unity characterizes the non-Newtonian behavior of fluid. In Power Law model, n is less than 1 implies its shear thinning ability. Moreover, n equals to 1 implies Newtonian fluid, whereas n is larger than 1 represents dilatant fluid.

2.2.2.3 Yield Power Law

Yield Power Law model, also called Herschel-Bulkley, and yield pseudoplastic model, combines the Bingham Plastic and Power Law model behavior. It requires three parameters.

$$\tau = \tau_y + K\gamma^n \tag{2-4}$$

The model has yield stress parameter, τ_y, as in Bingham Plastic model that is used to represent the threshold stress to flow initialization. Moreover, it has consistency index, K, and flow behavior index, n, as in Power Law model. YPL model can represent Newtonian fluids, Bingham Plastic and Power Law fluids. Input of $n = 1$, $K = \mu$, and $\tau_y = 0$ becomes Newtonian fluid; $n = 1$, and $\tau_y = 0$ indicates Power Law fluid; and $K = \mu_p$, $\tau_y = YP$, and $n = 1$ implies Bingham Plastic fluid.

Yield Power Law model is an accurate model for most of the drilling fluids due to represent its shear thinning ability and yield stress. It accurately captures the drilling fluid behavior at high and low shear rates.

CHAPTER 3

STATEMENT OF THE PROBLEM

3.1 Statement of the Problem

During drilling, pulling or slacking the drillstring, significant pressure changes at the wellbore may occur. These pressure changes can disturb the desired pressure balance at the bottomhole or anywhere in the open hole section. It is important to accurately estimate the swab and surge pressures to avoid any hazardous situation. Accurate estimation of swab and surge pressures will help optimizing the tripping operation to trip in or out as fast as possible while staying in the mud window between the pore and fracture pressure.

There are several published models on modeling surge and swab pressures in concentric annuli. Yet, very limited work is conducted on surge and swab pressures of Yield Power Law fluids. YPL fluids better represent the behavior of the current drilling fluids. Moreover, most of the models in literature approximate the annulus as a narrow slot, which is not necessarily accurate at low diameter ratios. Accurate calculation of the equivalent circulating density (ECD) variation due to surge and swab pressure changes is the main objective of this study. With this, it is expected that safe and optimized tripping operations can be commenced.

3.2 Objectives and Approach

The major objectives of this study are:

- To develop a mathematical model that predicts the swab and surge pressures of Newtonian fluids in concentric annuli
- To develop a mathematical model that predicts the swab and surge pressures of YPL fluids in concentric annuli
- To conduct a CFD analysis of swab and surge pressures of Newtonian fluids to validate the mathematical model
- To run the validated mathematical model with various diameter ratio, flow behavior index and pipe speed to understand the effects on the swab and surge

The governing equations for the flow in annuli due to reciprocation of the inner pipe is obtained by simplifying the Navier-Stokes equations. Non-Newtonian fluids, (YPL model) is considered at the definition of the shear stress and it is included to the governing equations, as the details are given at the following chapters of this thesis.

Finite difference method is applied to the partial differential equations and an iterative finite difference scheme is developed to solve the equations. The developed mathematical model is validated with the CFD analysis conducted by a commercial CFD program (ANSYS FLUENT, ANSYS CFX v.14.0).

CHAPTER 4

SURGE AND SWAB PRESSURES OF NEWTONIAN FLUIDS IN CONCENTRIC ANNULI

4.1 Development of the Analytical Solution

Derivation for the swab and surge pressures of Newtonian fluids in concentric annuli is done within the scope of this study and presented in Appendix A. The derivation is based on the momentum balance and boundary conditions for a moving pipe in annular space, using Newtonian fluids.

The final form of the analytical solution is given below (Equation A-24).

$$v_z = \frac{\mathrm{dP}}{\mathrm{d}l}\frac{\left(r^2 - {R_i}^2\right)}{4\mu} - \left[\frac{\mathrm{dP}}{\mathrm{d}l}\frac{\left({R_o}^2 - {R_i}^2\right)}{4\mu} + v_p\right]\frac{ln\left(\frac{r}{R_i}\right)}{ln\left(\frac{R_o}{R_i}\right)} + v_p \qquad \text{(A-24)}$$

4.2 Development of the Numerical Solution

A numerical model that estimates the surge and swab pressures in concentric annuli is derived and presented in this study. The derivation of the numerical model can be found at Appendix B.

The final form of the numerical solution is presented in Equation B-15.

$$\frac{\partial p}{\partial z}2\Delta r^2 = \left(\left({\mu_{i+1}}^k + {\mu_i}^k + {\mu_i}^k\frac{\Delta r}{r}\right)({v_{i+1}}^{k+1})\right.$$
$$- ({\mu_{i+1}}^k + 2{\mu_i}^k + {\mu_{i-1}}^k)({v_i}^{k+1}) \quad \text{(B-15)}$$
$$\left. + \left({\mu_i}^k + {\mu_{i-1}}^k - {\mu_i}^k\frac{\Delta r}{r}\right)({v_{i-1}}^{k+1})\right)$$

An apparent viscosity needs to be defined since the fluid is non-Newtonian. Viscosity terms in Equation B-15 will be replaced with μ_{app}.

$$\mu_{app} = \frac{\tau}{\gamma} \quad \text{(B-16)}$$

In which YPL defines τ as:

$$\tau = \tau_0 + K\gamma^n \quad \text{(B-17)}$$

Apparent viscosity function for YPL fluids can be defined as:

$$\mu_{app} = \frac{\tau_0}{\gamma} + K\gamma^{n-1} \quad \text{(B-18)}$$

Where shear rate function given as:

$$\gamma = \frac{\partial v_r}{\partial z} \quad \text{(B-19)}$$

The modeling work includes simplifying the Navier-Stokes equation to the governing equations for the surge and swab pressures in concentric annuli under certain assumptions. The assumptions are also listed in the Appendix B. The numerical model includes a finite difference approximation and a numerical scheme that can calculate frictional pressure losses for the given input parameters, i.e. the fluid properties, fluid density, etc. To solve the scheme iteratively, a MATLAB code is written within the scope of this study. The input parameters are listed in flow chart (Figure 4-1) that represents the numerical scheme that is proposed with this study.

Using this, the velocity profile for a given pressure value is calculated. In order to obtain the pressure for a given average velocity, a root finding algorithm is used. In this study, MATLAB's fzero() function is used, which is a combination of secant, bisection and inverse quadratic interpolation methods that enables finding the pressure losses for a given velocity (Forsythe et al., 1977).

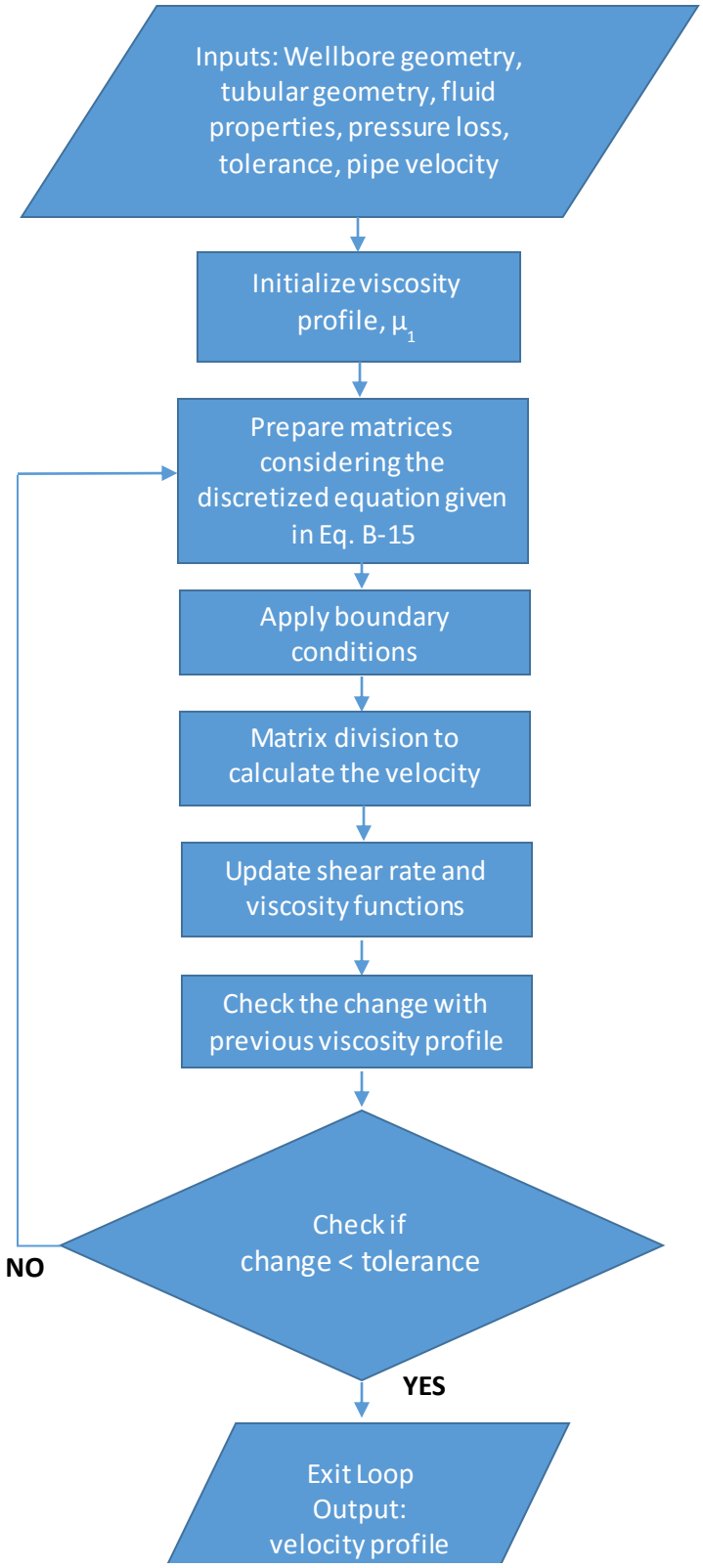

Figure 4-1. Flow Diagram of Numerical Model Solution

4.3 CFD Analysis

Computational Fluid Dynamics (CFD) is the science of simulating flow related problems using computer resources. It provides qualitative and quantitative predictions of fluid flow, mass transfer, heat transfer and related phenomena by solving mathematical equations. To address the fluid problem, first, it is needed to know physical properties of fluid system. Then, the analysis continues with a mathematical model of the physical problem (partial differential equations). Some certain assumptions are needed to be made in order to simplify and eventually make the problem tractable. The PDE should be transformed into discretized form using numerical discretization methods, such as Finite Difference, Finite Element, or Finite Volume methods. The domain needs to be divided into smaller discrete volumes, called mesh generation, for better analysis. The number of cells and node requirement is needed to be set for each geometry. Collection of cells or grids, must be sufficiently fine to accurately resolve the flow problem. After setting initial and boundary conditions, the set of equations are solved numerically for each cell. The equations are solved simultaneously and iteratively to provide a solution. Finally, the solution is post-processed in order to obtain the desired quantities at desired location. Graphical results such as animations, contours, vector plots, XY plots, particle trajectory plots, and numerical results, such as velocity profiles, forces, pressure gradients are compared and analyzed in desired way. The simulation results can show how fluid flow, particle flow, chemical reactions, combustion, heat transfer and other parameters evolve with time. Figure 4-2 shows the process of computational fluid dynamics.

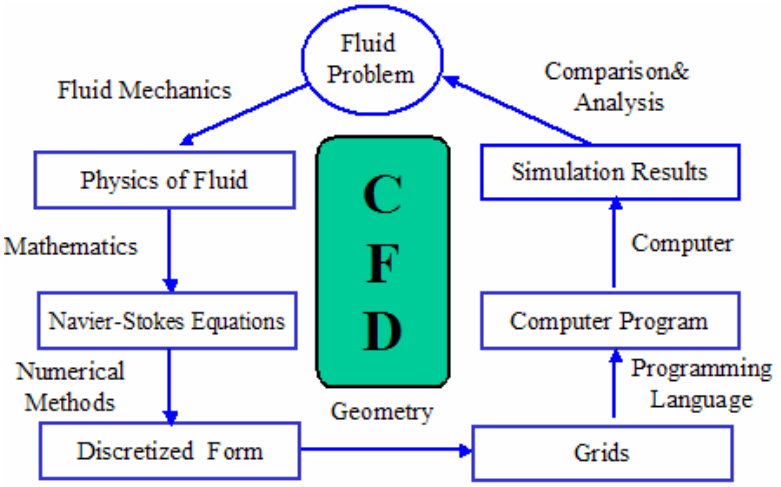

Figure 4-2. Process of Computational Fluid Dynamics (Zuo, 2005)

In this study, commercial CFD softwares, ANSYS Fluent, and ANSYS CFX are used to simulate the flow in the annuli while reciprocating the inner pipe, which is seen during tripping operation of well construction process. Fluent uses a cell-centered finite volume solution, in which the flow variables are stored at the center of the mesh elements. CFX has a solution method, which uses cell-vertex finite volume technique, flow variables of which are stored at the vertices of grids (ANSYS, 2013).

In this subsection, all of the analysis conducted using ANSYS FLUENT v. 14.0, is presented. At section 4.4 the runs with ANSYS CFX are also presented.

The inputs to the CFD software are summarized in Table 4-1.

Table 4-1. Input Parameters used to Simulate Flow in CFD Software

Geometry	R_i	0.016764 m
	R_o	0.0254 m
	L	3 m
Mesh	Minimum Size	1e-05
	Maximum Face Size	1e-03
	Maximum Size	1e-03
	Nodes	4328884
	Elements	3928309
Set-up and Solution	Water Density @ 25°C	1000 kg/m^3
	Water Viscosity @ 25°C	0.001 kg/ms
	Minimum Orthogonal Quality	0.898865
	Maximum Aspect Ratio	2.63747

4.3.1 Geometry

3 meters long fluid body in the shape of an annular geometry is considered. Outer diameter of the pipe corresponds to borehole wall and inner diameter of pipe is the outer diameter of tubular in hole. The thickness of pipe is the fluid in the annulus. The geometry, dimensions and the details of the circular tube can be seen in Figure 4-3, Figure 4-4, and Figure 4-5 respectively.

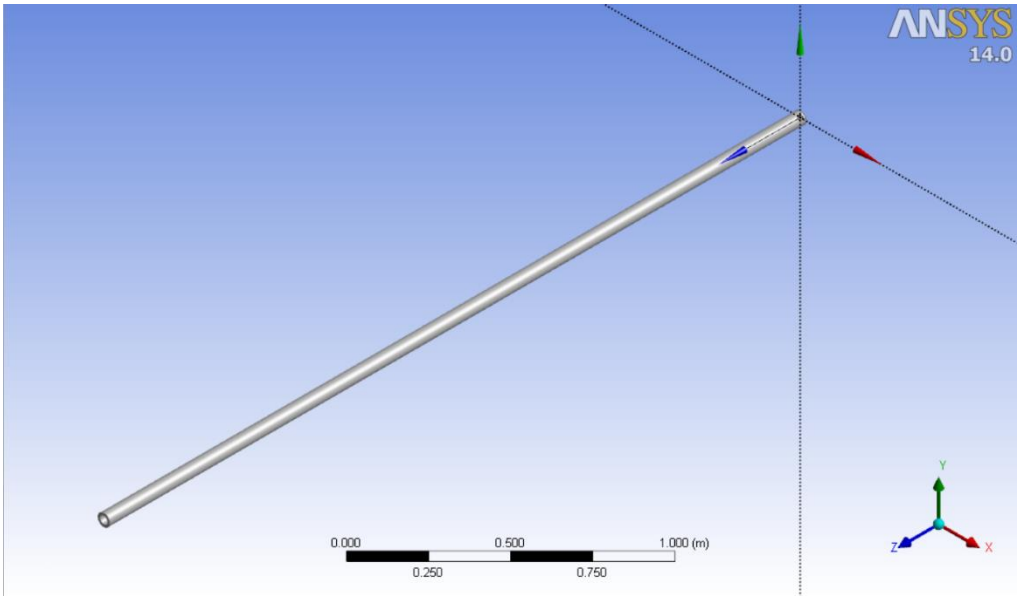

Figure 4-3. Isometric view of the geometry

Details View

Details of CircularTube1	
Sketch	CircularTube1
Show Constraints?	No
Dimensions: 2	
Ri	0.016764 m
Ro	0.0254 m
Edges: 2	
Full Circle	Cr9
Full Circle	Cr10
Physical Properties: 6	
(A)	0.0011439 m^2
(Ixx)	2.6488e-007 m^4
(Iyy)	2.6488e-007 m^4
(J)	5.2976e-007 m^4
(CGx)	0 m
(CGy)	0 m

Figure 4-4. Dimensions of Geometry

Details View

Details of Body	
Body	Fluid
Volume	0.0034318 m^3
Surface Area	0.79706 m^2
Faces	4
Edges	4
Vertices	0
Fluid/Solid	Fluid

Figure 4-5. Details of Fluid Body

4.3.2 Meshing

In meshing section, the domain is divided into discrete volumes. Also, boundaries are positioned and named. Figure 4-6 shows the details of the mesh.

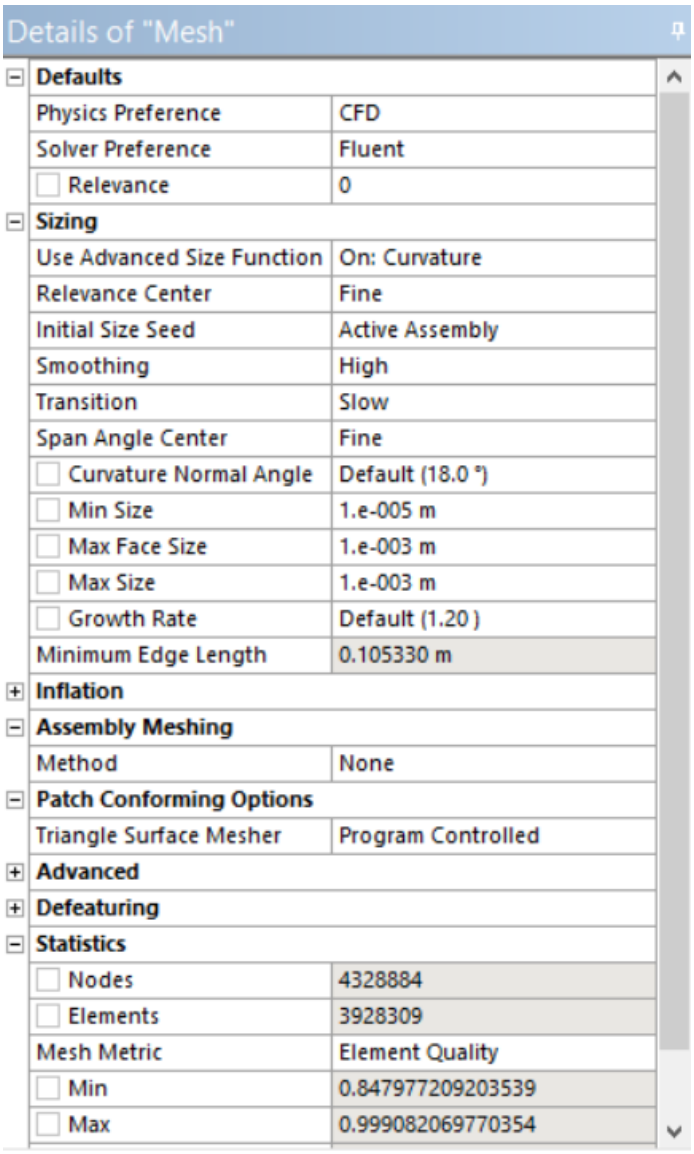

Details of "Mesh"

Defaults	
Physics Preference	CFD
Solver Preference	Fluent
Relevance	0
Sizing	
Use Advanced Size Function	On: Curvature
Relevance Center	Fine
Initial Size Seed	Active Assembly
Smoothing	High
Transition	Slow
Span Angle Center	Fine
Curvature Normal Angle	Default (18.0 °)
Min Size	1.e-005 m
Max Face Size	1.e-003 m
Max Size	1.e-003 m
Growth Rate	Default (1.20)
Minimum Edge Length	0.105330 m
Inflation	
Assembly Meshing	
Method	None
Patch Conforming Options	
Triangle Surface Mesher	Program Controlled
Advanced	
Defeaturing	
Statistics	
Nodes	4328884
Elements	3928309
Mesh Metric	Element Quality
Min	0.847977209203539
Max	0.999082069770354

Figure 4-6. Details of Mesh

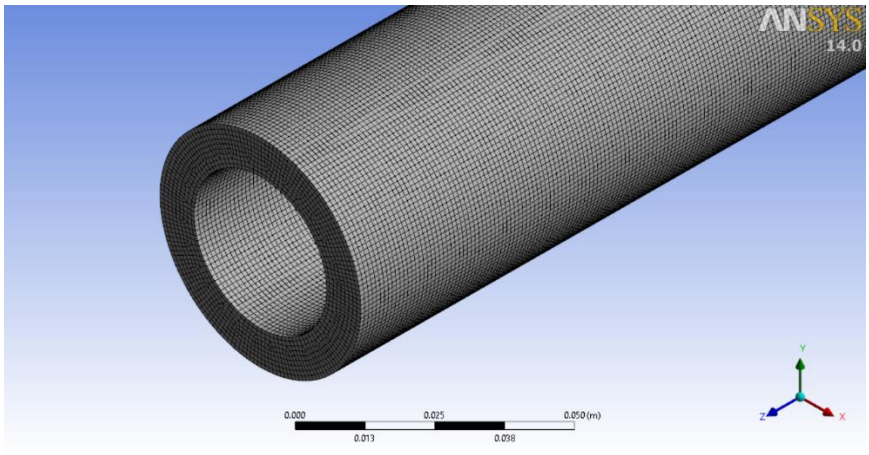

Figure 4-7. Isometric View of Mesh

Figure 4-7 shows the discrete volumes, grids, maximum size of which is 0.001 meters. The positions and names of boundary settings of the geometry is shown in Figure 4-8, Figure 4-9, and Figure 4-10.

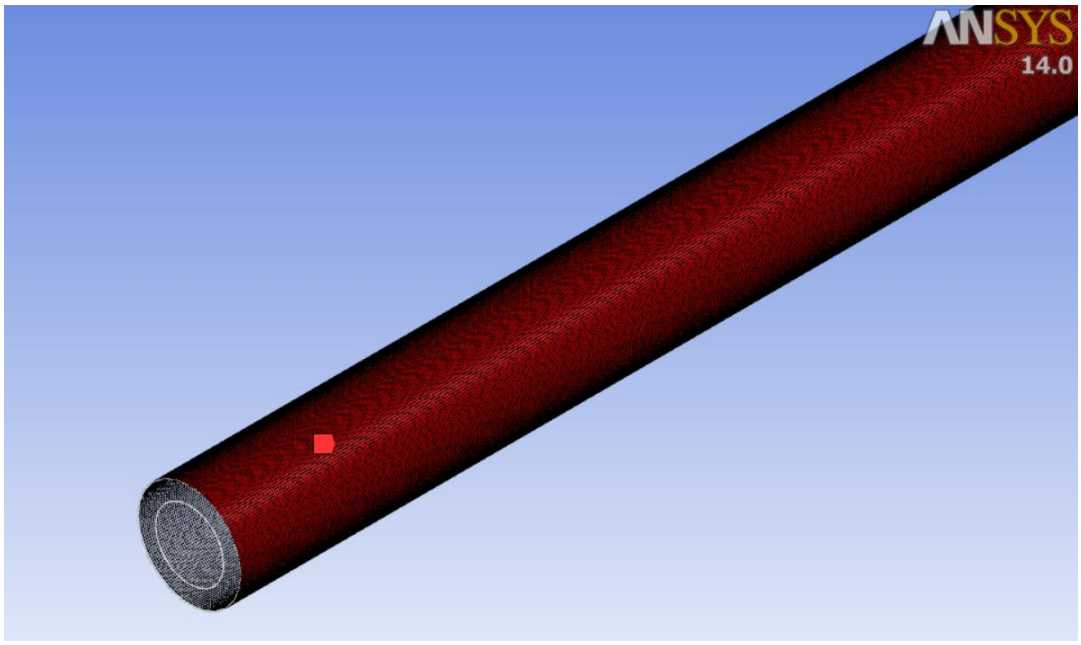

Figure 4-8. Outer Wall

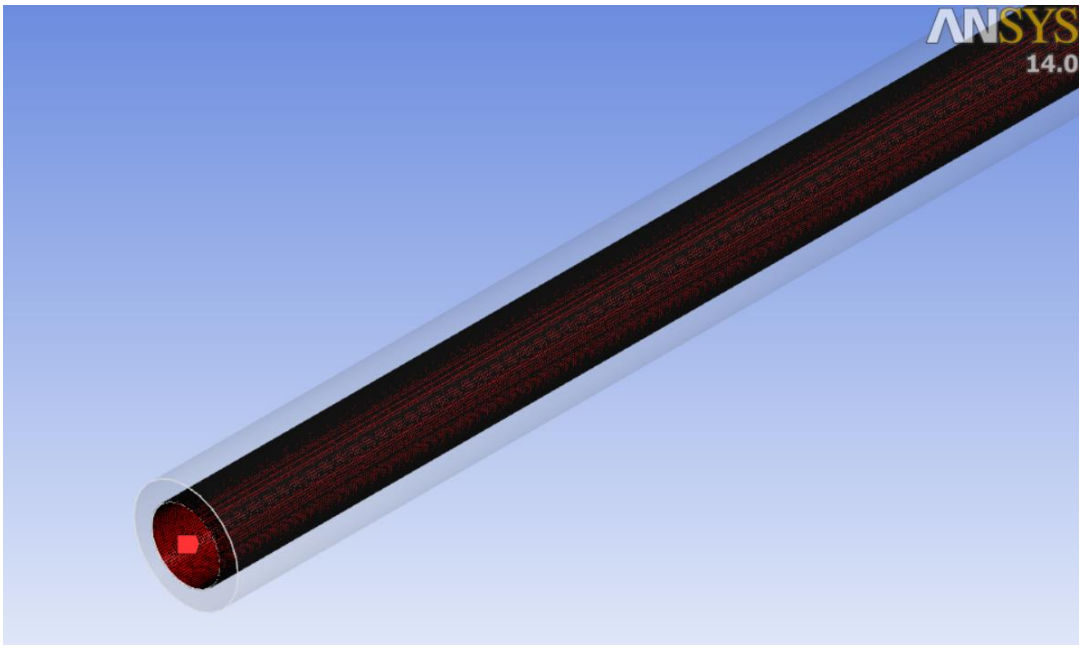

Figure 4-9. Reciprocating Wall

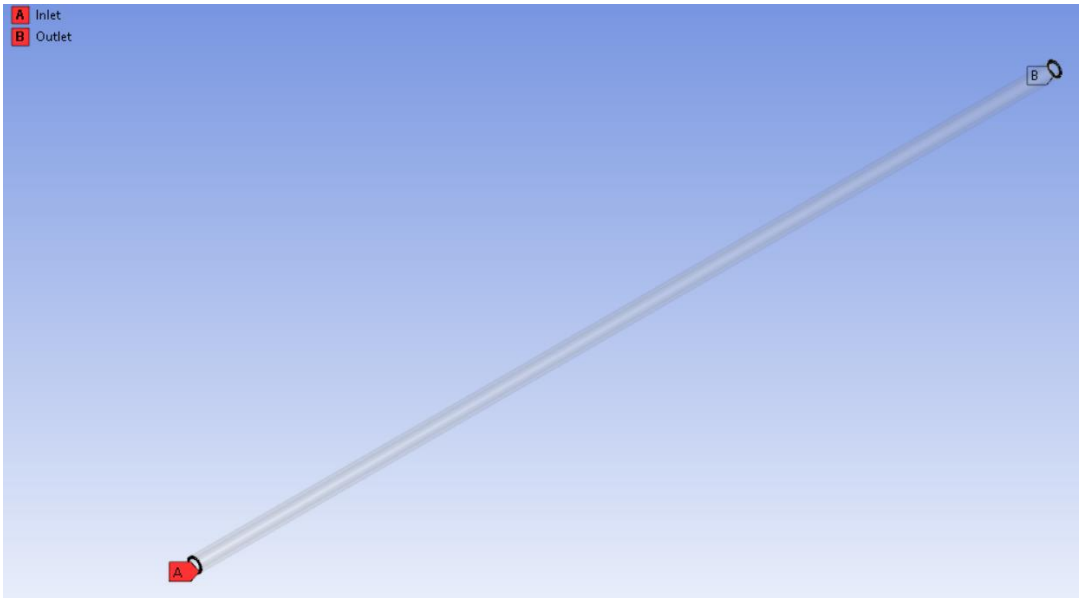

Figure 4-10. Inlet and Outlet

4.3.2.1 Grid Independence Study

In CFD analyses, it is needed to conduct grid independence study in order to ensure that the solution of CFD problem is independent from the grid size. It is better to maintain the lowest grid count possible to both ease the simulation time and keep the accuracy of solution at the same time.

In this study, same analysis is conducted using different mesh sizes and the velocity profile results are compared with the results obtained from analytical model presented in Appendix A. Mesh #1 has the lowest element count, means the coarsest mesh. Element number increases from Mesh #1 to Mesh #5. The relative errors for each mesh size and absolute average percent errors are calculated using Equation 4-1 and 4-2, and the results are listed in Table 4-2.

$$Error_{Absolute} = \left| \frac{v_{CFD} - v_{Analytical}}{v_{Analyitcal}} \, x \, 100 \right| \tag{4-1}$$

$$Absolute\ Average\ Percent\ Error = \frac{1}{n}\left(\sum_{i=1}^{n} \left(Error_{Absolute,i} \right) \right) \tag{4-2}$$

Table 4-2. Various Mesh Sizes Used in the Grid Independence Investigation

	Node Size	Element Size	Average Absolute Percent Error
Mesh #1	36792	24990	10185.64
Mesh #2	175648	133598	75.93
Mesh #3	618280	522929	52.53
Mesh #4	4328884	3928309	3.63
Mesh #5	5634605	5206764	4.41

From Figure 4-11 and Table 4-2, it is seen that the errors in the Mesh #1, Mesh #2, and Mesh #3 are not sufficient and give highly erroneous results. For the sake of simplicity, an absolute average percent error of less than five percent is considered as the pass criteria. Mesh #4 and Mesh #5 are in the acceptable range. Note that the absolute average percent error is calculated over the velocity profiles, so the error would be significantly less in terms of pressure obtained with that particular velocity profile. The fine case, Mesh #5, has more cells to solve iteratively than the other runs. However, the coarser run, Mesh #4, has accurately established the velocity field. Therefore, the CFD solution using Mesh #4 is used in this study. The velocity profile comparison figures for CFD solution with each mesh size and analytical solution are given from Figure 4-12 to Figure 4-16:

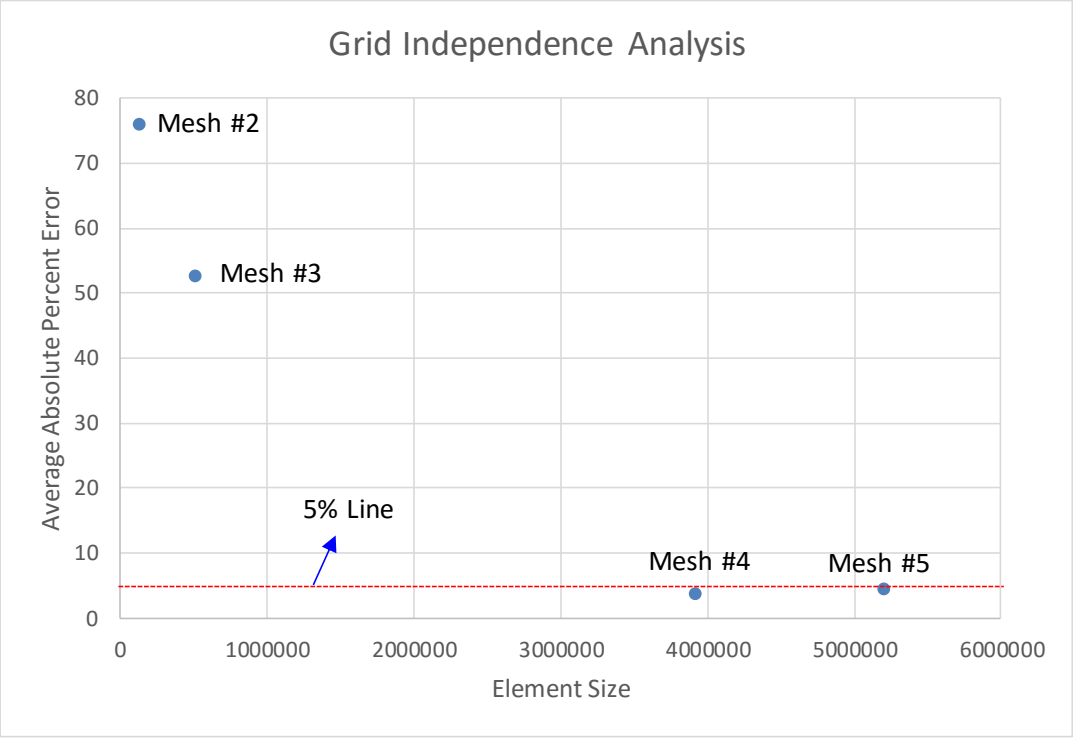

Figure 4-11. Grid Independence Analysis

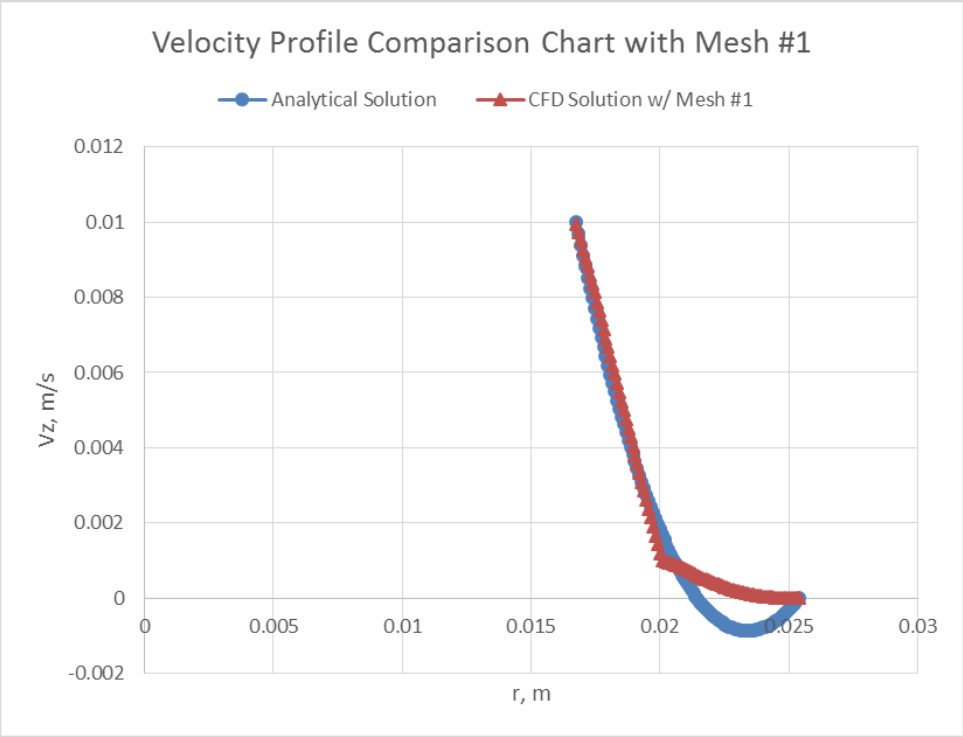

Figure 4-12. Velocity Profile Comparison between Analytical and CFD Solution with Mesh#1

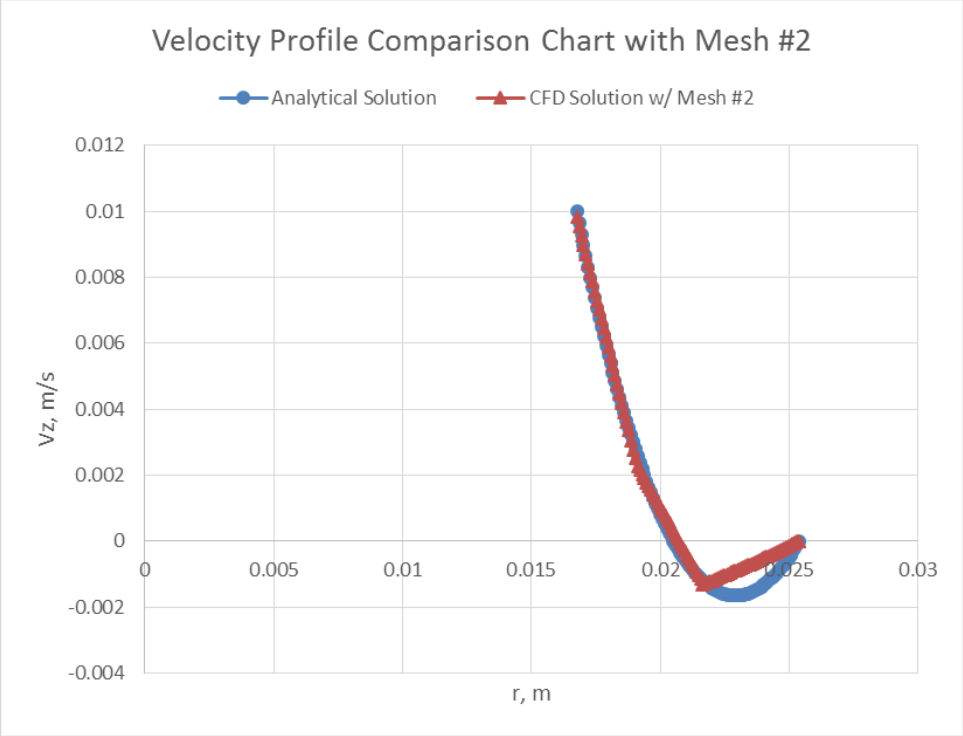

Figure 4-13. Velocity Profile Comparison between Analytical and CFD Solution with Mesh#2

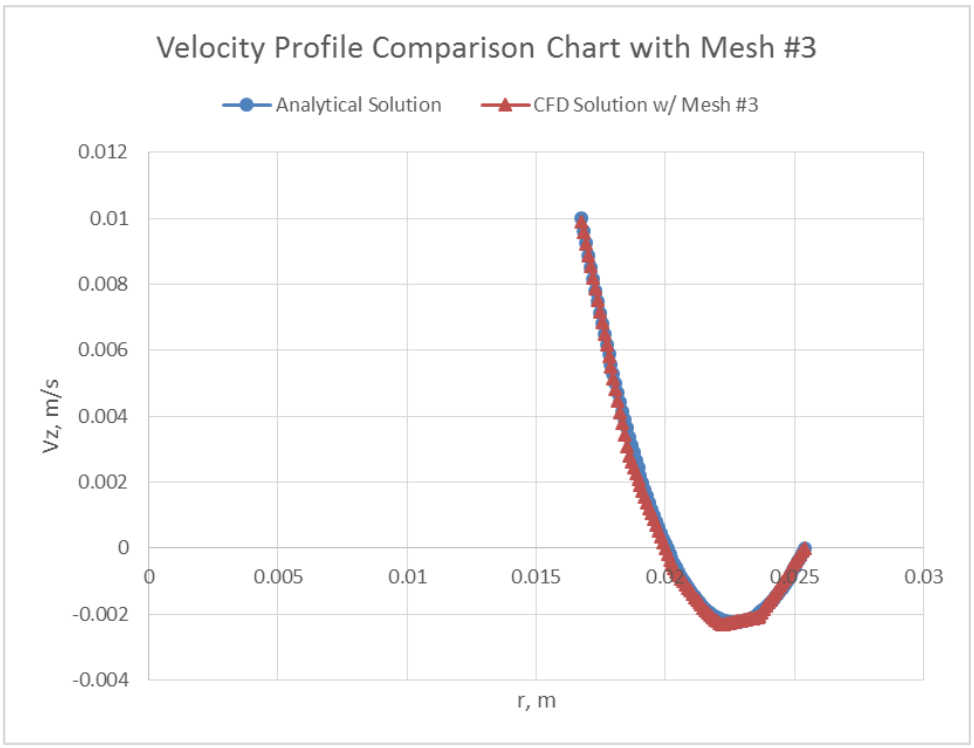

Figure 4-14. Velocity Profile Comparison between Analytical and CFD Solution with Mesh#3

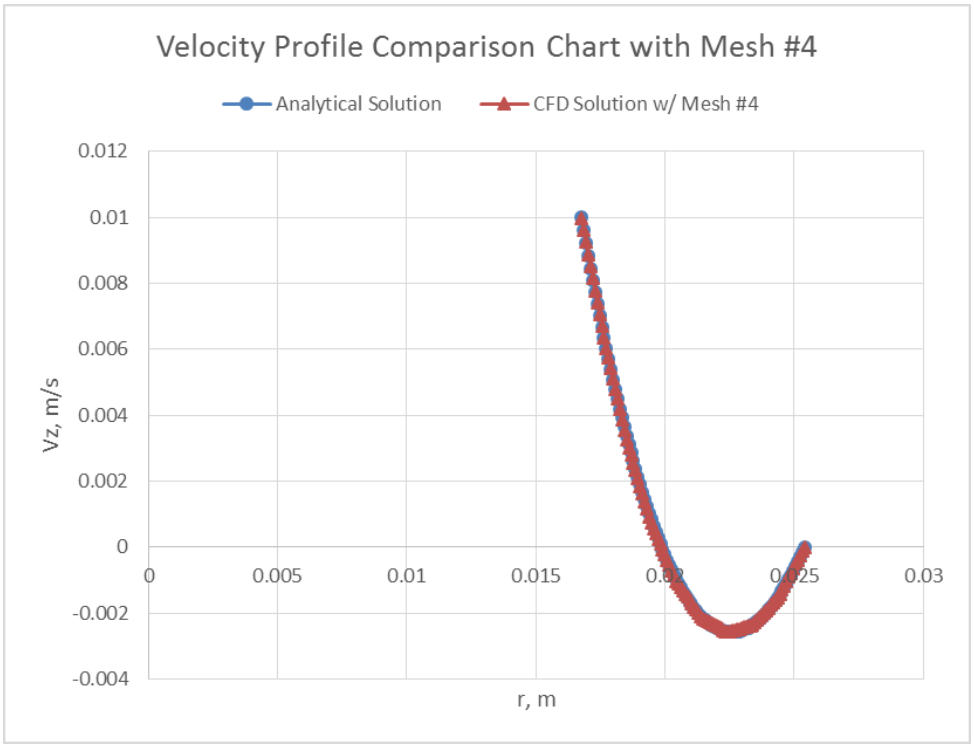

Figure 4-15. Velocity Profile Comparison between Analytical and CFD Solution with Mesh#4

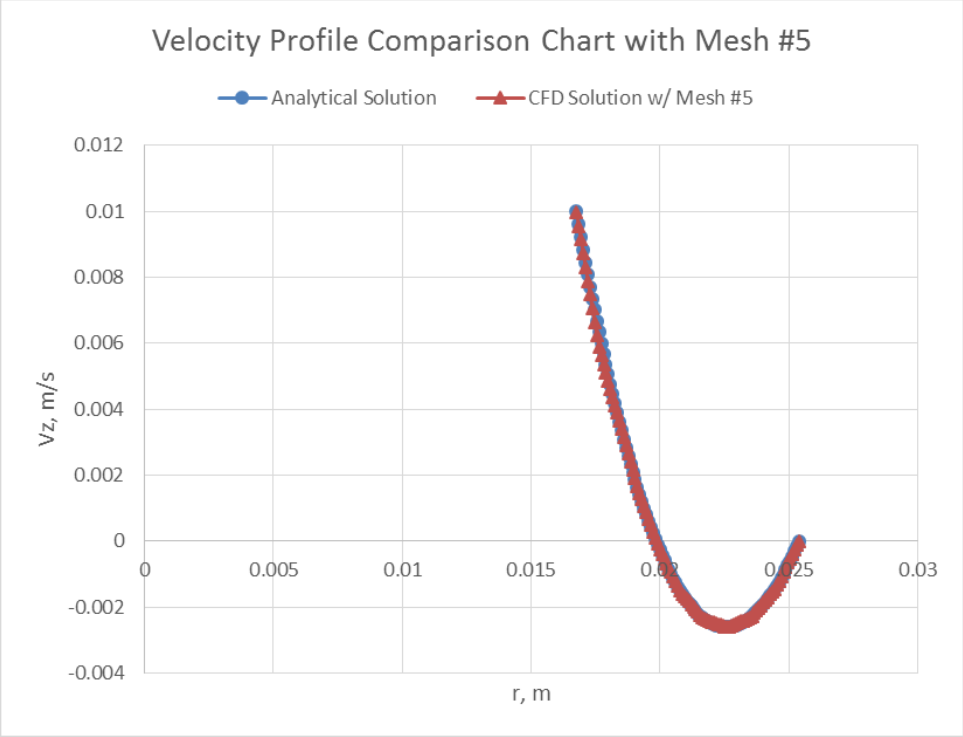

Figure 4-16. Velocity Profile Comparison between Analytical and CFD Solution with Mesh #5

4.3.3 Set-up and Solution

In this section, the drilling fluid properties, in this case water properties, are input as shown in Table 4-1. General solver settings, solution models and boundary conditions are set according to the assumptions listed in Appendix A. Corresponding figures can be seen from Figure 4-17 to Figure 4-19.

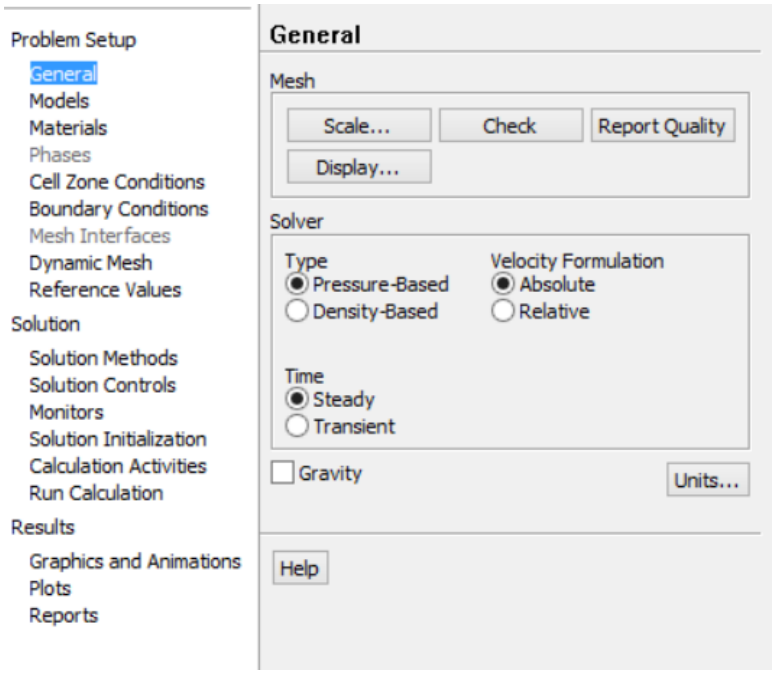

Figure 4-17. General Solver Settings

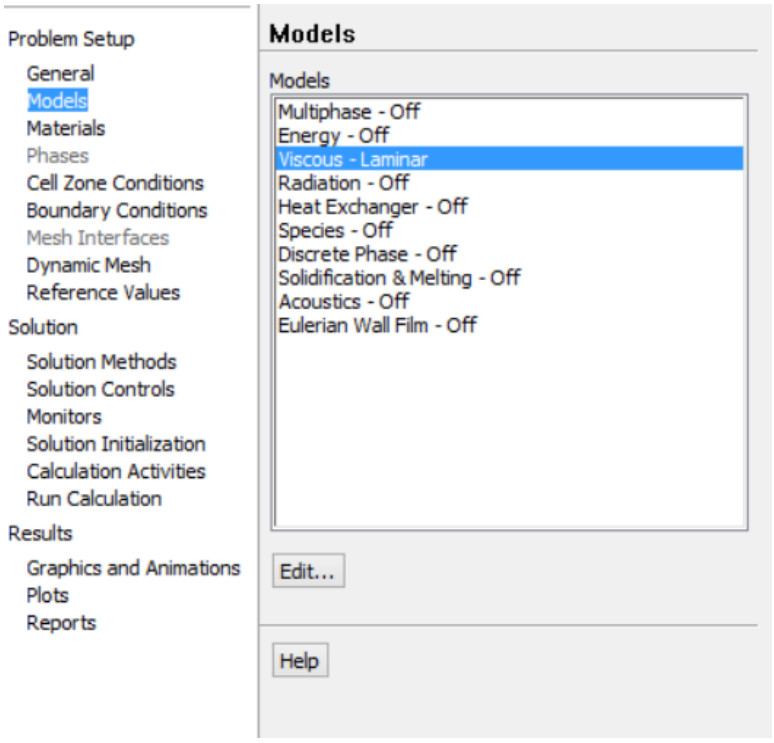

Figure 4-18. Solution Models

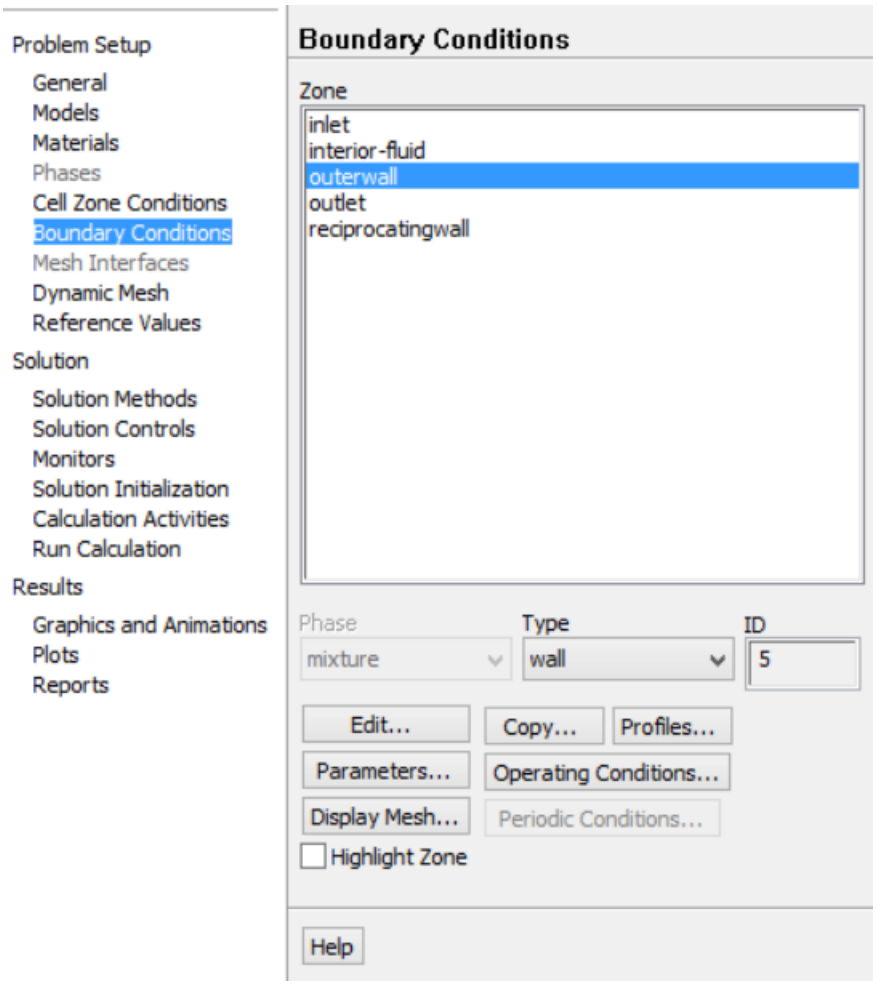

Figure 4-19. Boundary Conditions

The borehole wall is set as stationary outer wall, and inner wall is set as the reciprocating wall.

4.3.4 CFD Results

After numerical analysis by ANSYS Fluent, results are obtained. In this study, velocity values for desired data points are acquired and plotted with respect to varying radius, r. Velocity streamline of the analysis can be seen in Figure 4-20.

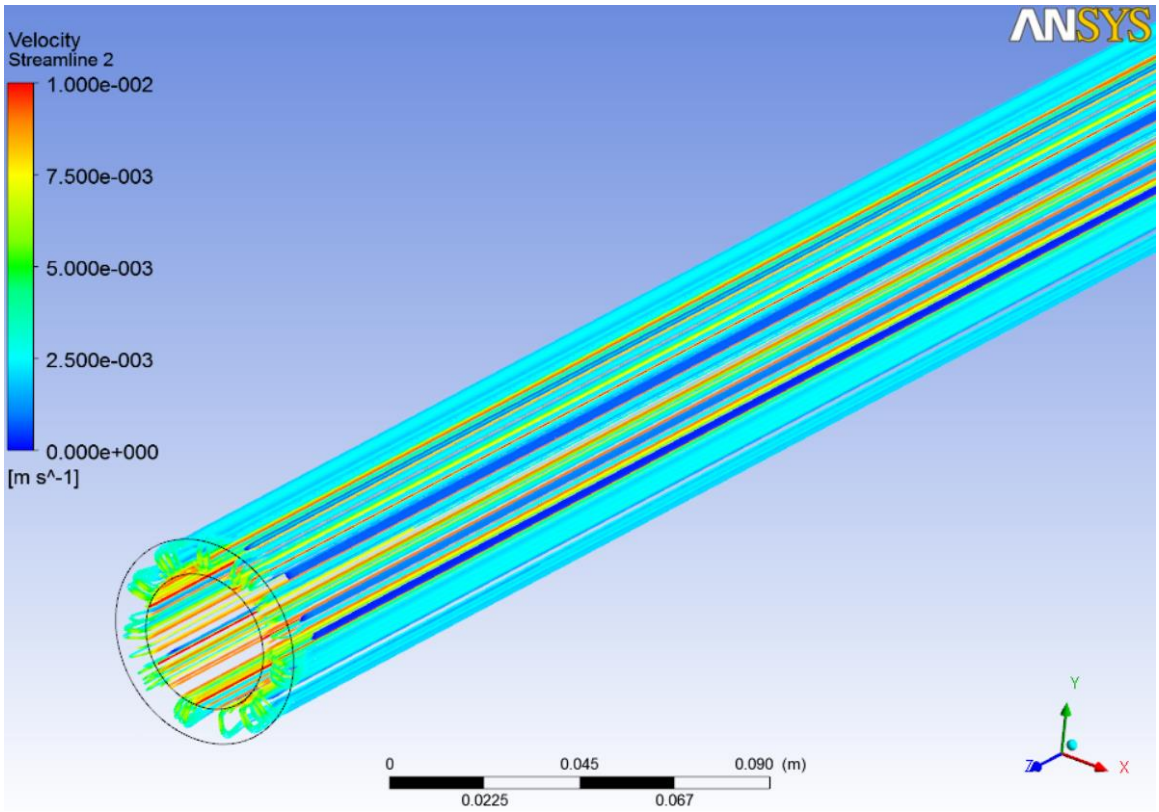

Figure 4-20. Velocity Streamlines Along the z- axis

4.4 Comparison between the Numerical Model, Analytical Solution and CFD Analysis

In this section, a comparison between the numerical model, analytical solution and the CFD analysis is presented. The aim of comparing the numerical model with the analytical solution and the CFD analysis is to validate the accuracy of the proposed numerical model. The derived analytical solution has been compared with the one presented in Chin (2011), which is shown in Equation 4-3.

$$v(r) = \left[\frac{(R_o^2 - R_i^2)P_z}{(4\mu)} + V_\infty\right]\frac{\log_e\left(\frac{R_o}{r}\right)}{\log_e\left(\frac{R_o}{R_i}\right)} + (r^2 - R_o^2)\frac{P_z}{(4\mu)} \quad (4\text{-}3)$$

A very good match is obtained while comparing those equations. Moreover, the numerical model has also in very good accordance with the analytical solutions. Figure 4-21 shows the velocity profile comparison among numerical and analytical models derived in this study, analytical model that is taken from literature, and CFD analysis for swab condition.

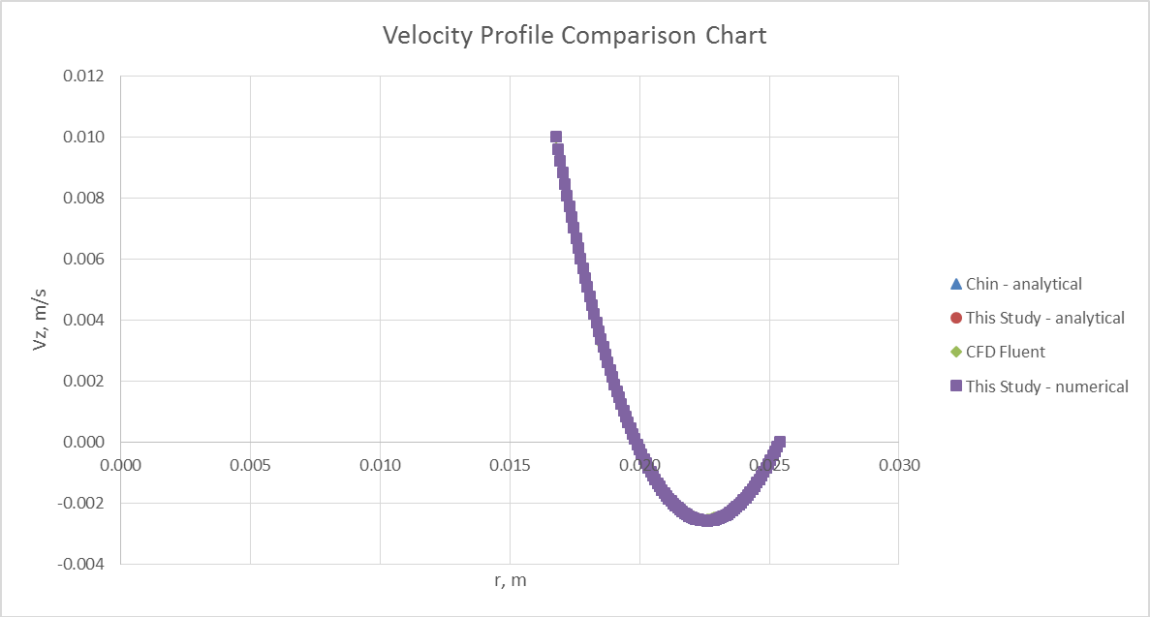

Figure 4-21. Velocity Profile Comparison between CFD, Numerical and Analytical Solution for the Newtonian Fluids while Moving the Tubular Upwards

At below Figure 4-22 and Figure 4-23, dimensionless velocity profile comparisons for swab and surge conditions are presented, respectively. Considering the solution and definition of dimensionless parameters, moving the pipe upwards or downwards should yield the same results and that is what we observe from these figures. The results are presented at the below figures:

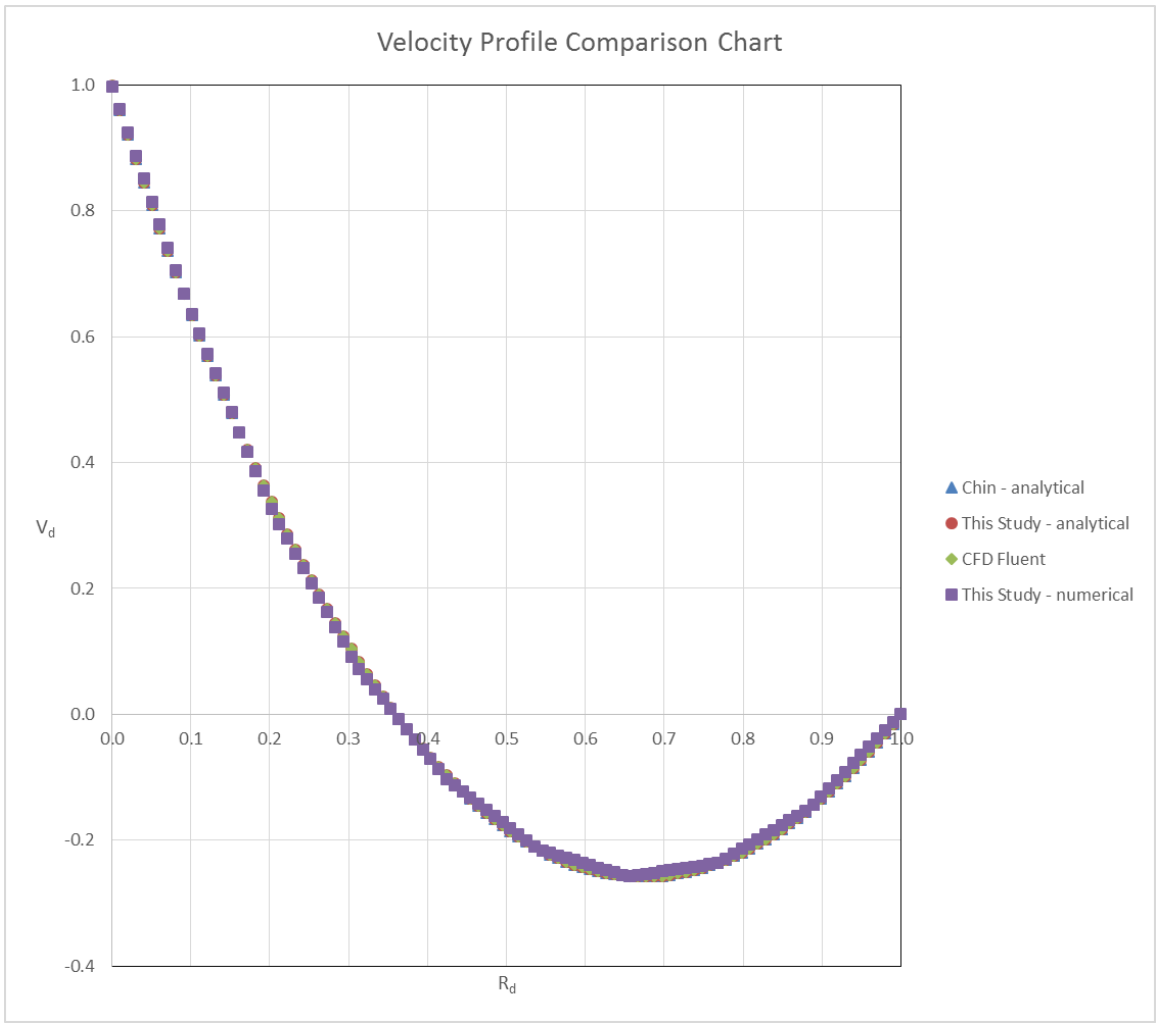

Figure 4-22. Dimensionless Velocity Profile Comparison between CFD, Numerical and Analytical Solution for the Newtonian Fluids while Moving the Tubular Upwards

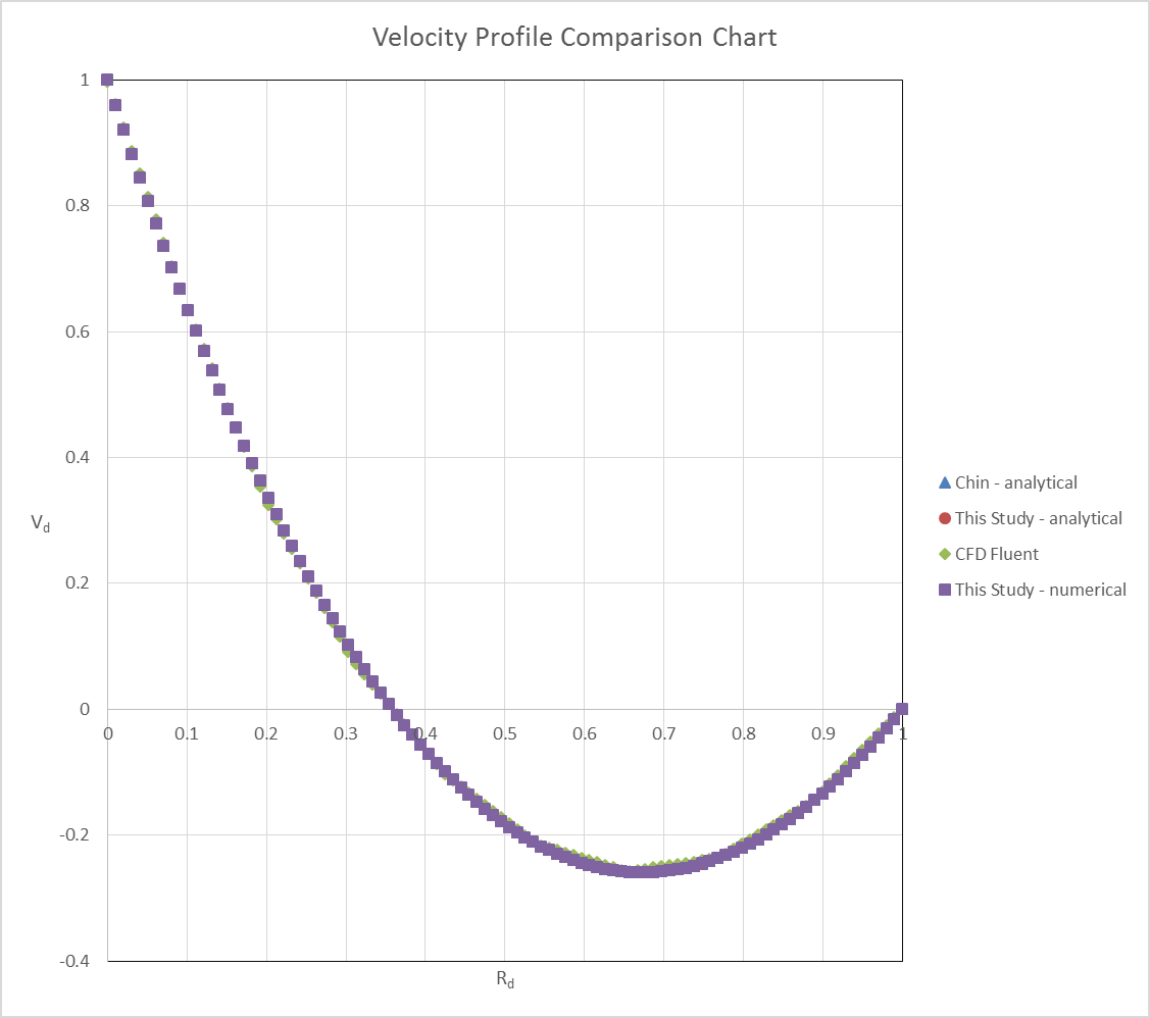

Figure 4-23. Dimensionless Velocity Profile Comparison between CFD, Numerical and Analytical Solution for the Newtonian Fluids while Moving the Tubular Downwards

Dimensionless velocity (V_d) is defined by taking the ratio of the local velocity (V_z) to the pipe's velocity (V_p).

$$V_d = \frac{V_z}{V_p} \tag{4-4}$$

Dimensionless radius (R_d) is defined as following:

$$R_d = \frac{(r - R_i)}{(R_o - R_i)} \tag{4-5}$$

As it can be seen in Figure 4-22 and Figure 4-23, the comparisons show a good agreement between the numerical model, analytical solution and the CFD analysis. This comparison demonstrates the capability of the proposed solution and how accurately it captures the velocity profile and pressure losses in a concentric annuli. This validated numerical scheme will be extended to incorporate the Yield Power Law fluids in the following chapters.

Since the dimensionless parameters are used in the comparison, the velocity profiles that are created by surge and swab conditions were the same. Therefore, in order to see the velocity profile while surge, an example velocity profile for the pipe moving downwards is presented at Figure 4-24, below.

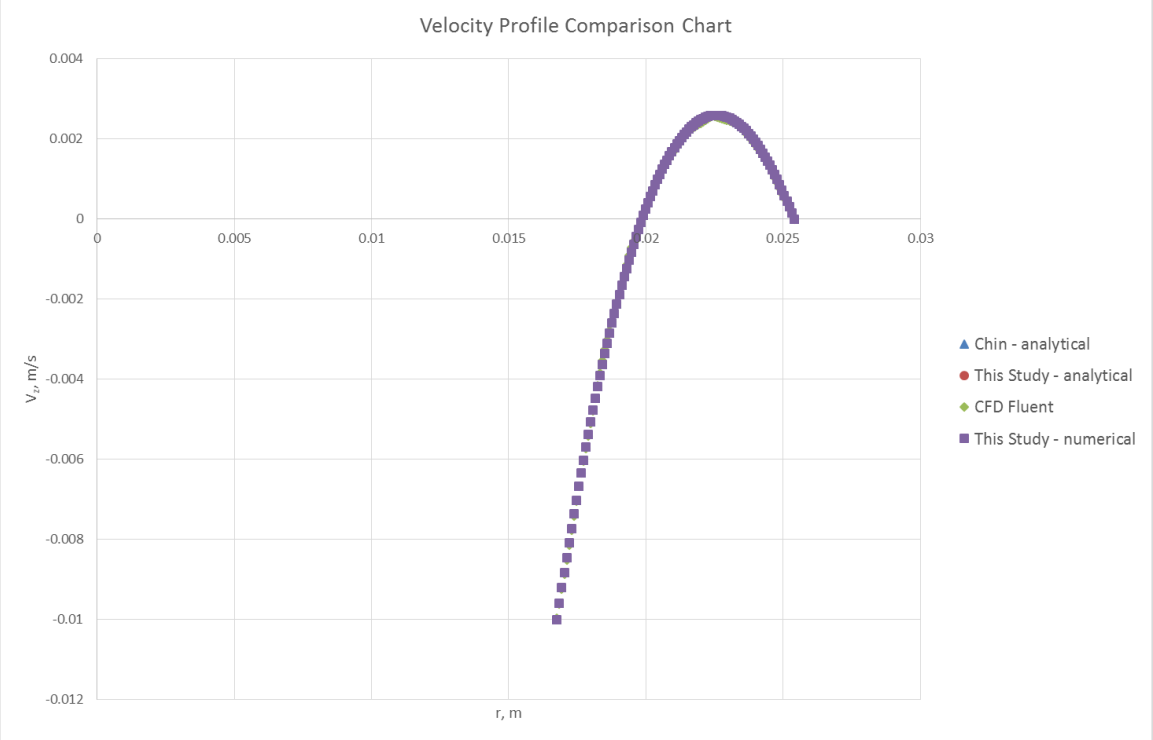

Figure 4-24. Velocity Profile Comparison between CFD, Numerical and Analytical Solution for the Newtonian Fluids while Moving the Tubular Downwards

A comparison between the analytical solution and another commercial CFD software ANSYS CFX v. 14.0 is presented in Figure 4-25. Similar to the previous results with FLUENT, a good agreement with the analytical solution and CFD results are obtained.

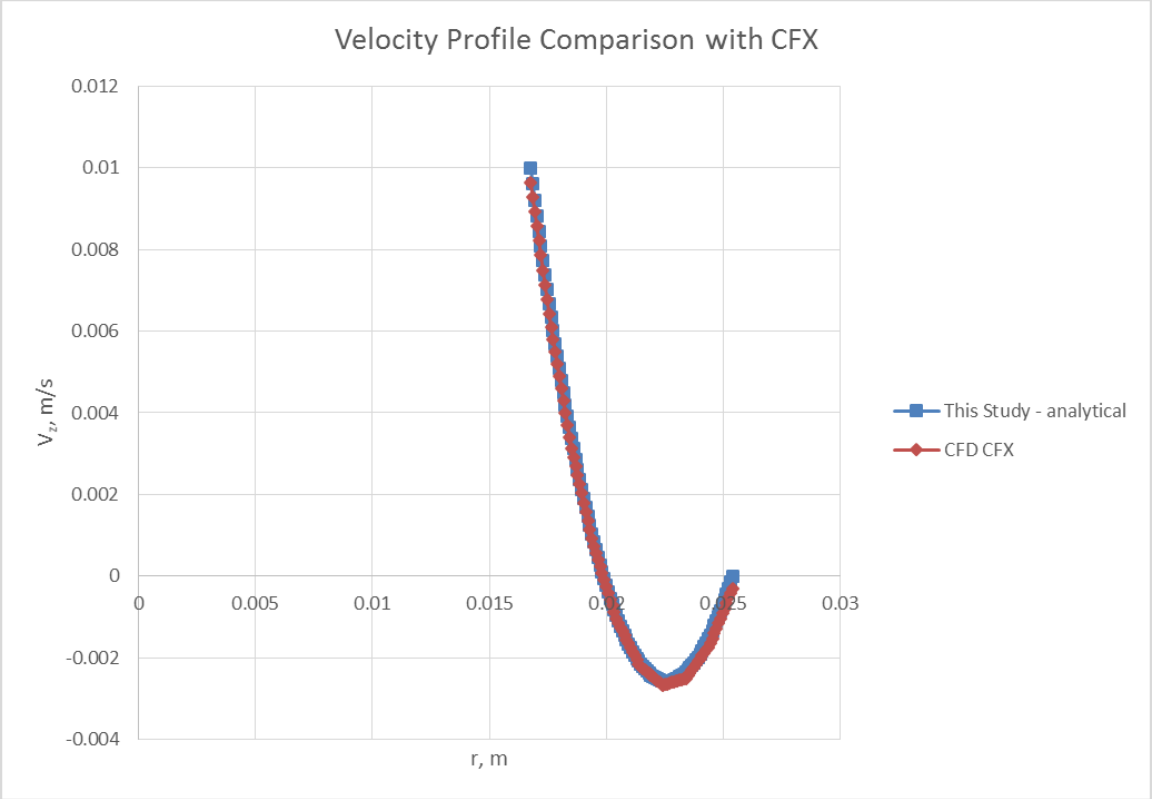

Figure 4-25. Velocity Profile Comparison between Analytical Solution and ANSYS CFX

4.5 Results and Discussions

In this section, the effect of diameter ratio, pipe velocity and viscosity on surge and swab pressure are investigated. The numerical algorithm is ran with various parameters to understand the sensitivity of the surge and swab pressure of Newtonian fluids with changing diameter ratio, pipe velocity and viscosity. Base input parameters while conducting sensitivity analysis for Newtonian fluids are listed in Table 4-3.

Table 4-3. Inputs of Numerical Analysis for Newtonian Fluid

Input Parameters - Newtonian	
μ	0.9 Pa.s
V_p	0.1 m/s
R_o	0.31115 m
R_i	0.2032 m
R_i/R_o	0.653
ρ	1000 kg/m^3

4.5.1 Effect of Diameter Ratio

Figure 4-26 illustrates the effect of diameter ratio on surge and swab pressure gradient with varying dynamic viscosity values. It can be seen that an increase in aspect ratio results in increase in surge and swab pressure gradients. It is observed from Figure 4-26 that as the value of diameter ratio increases, pressure losses tend to increase exponentially after a certain point, due to the natural logarithmic relationship between diameter ratio and pressure losses. Moreover, the effect gets more pronounced with fluids that have high viscosity.

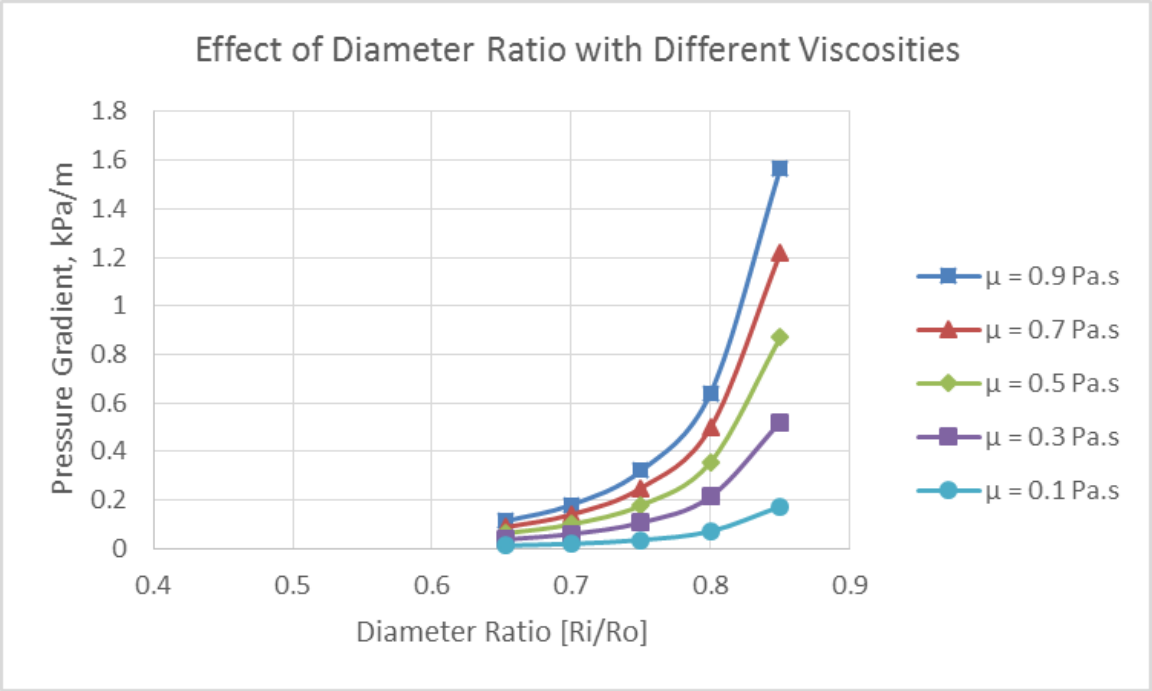

Figure 4-26. Effect of Diameter Ratio with Different Viscosity Values on Surge and Swab Pressure Gradient for Newtonian Fluid

4.5.2 Effect of Pipe Velocity

As expected, increasing the velocity of drillstring increases the resulting surge or swab pressures as shown in Figure 4-27. Additionally, velocity increase seems to increase the pressure change in the bottomhole exponentially with increase in diameter ratio.

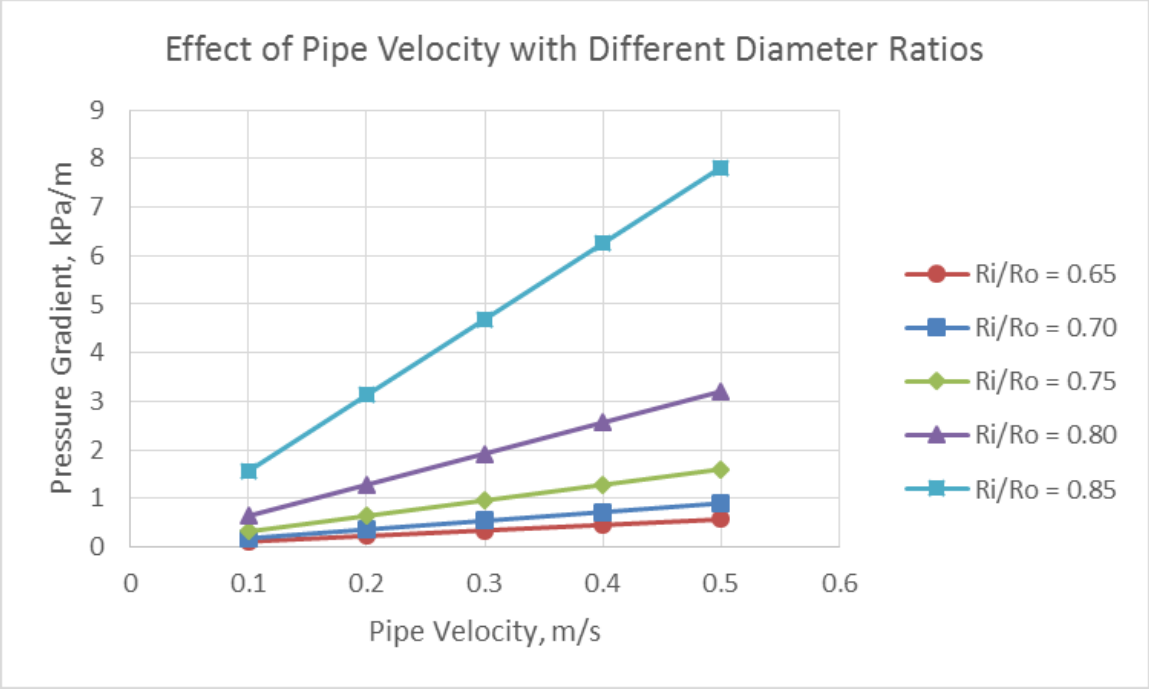

Figure 4-27. Effect of Pipe Velocity with Different Diameter Ratios on Surge and Swab Pressure Gradient for Newtonian Fluid

4.5.3 Effect of Viscosity

As Figure 4-28 illustrates, the pressure change in the hole with axial motion of drillstring has a direct proportionality with the viscosity of Newtonian fluids. Same relationship can be seen with pipe velocity with a linear rate.

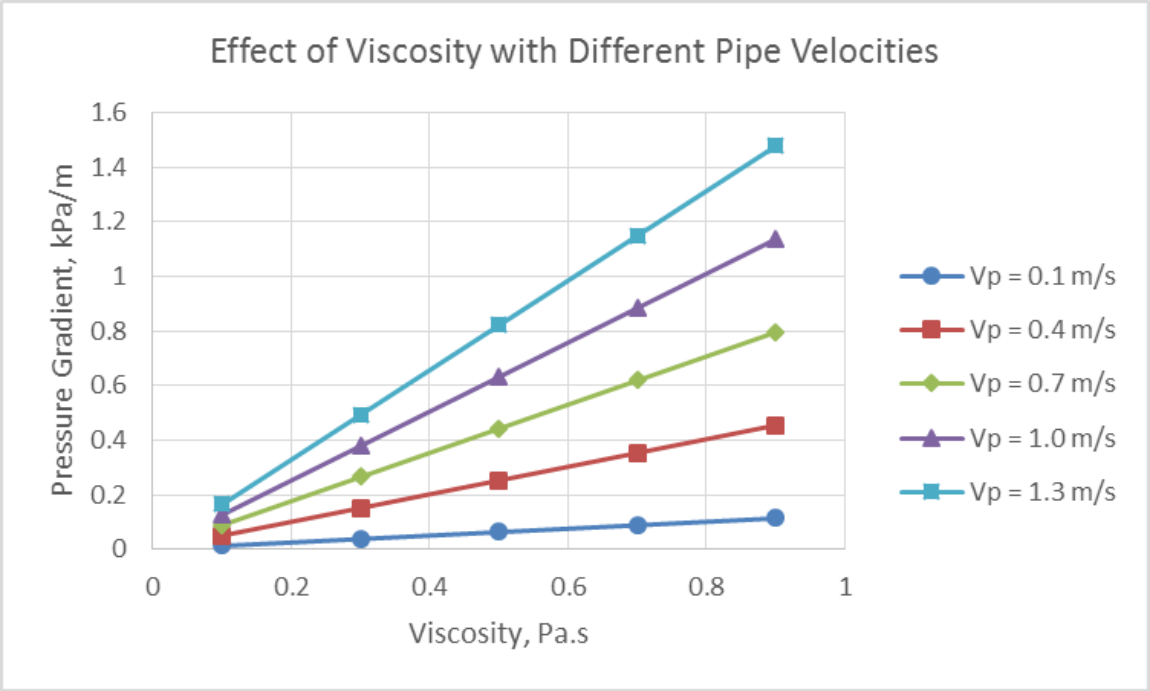

Figure 4-28. Effect of Viscosity with Different Pipe Velocities on Surge and Swab Pressure Gradient for Newtonian Fluid

CHAPTER 5

SURGE AND SWAB PRESSURES OF YIELD POWER LAW FLUIDS IN CONCENTRIC ANNULI

5.1 Development of the Numerical Solution

The proposed numerical solution at the previous chapter is extended for the Yield Power Law fluids. An apparent viscosity function is defined and applied to the numerical scheme to enable Yield Power Law fluid behavior. The equation and the derivation of the numerical scheme is presented in the previous chapter and in Appendix B.

5.2 Results and Discussion

In this section, the effect of diameter ratio, pipe velocity, yield stress and generalized flow behavior index on surge and swab pressure are investigated. The results are presented in the following subsections. The input parameters listed in Table 5-1 are used in this sensitivity analysis, unless stated otherwise.

Table 5-1. Inputs of Numerical Analysis for YPL Fluid

Input Parameters - YPL	
K	0.5 Pa.s
V_p	0.1 m/s
R_o	0.31115 m
R_i	0.2023 m
R_i/R_o	0.65
ρ	1000 kg/m^3
τ_y	2 Pa
n	0.5

5.2.1 Effect of Diameter Ratio

Figure 5-1 shows the effect of diameter ratio on surge and swab pressure gradients with different yield stress values for YPL fluids. Increasing the diameter ratio results in an increase in the pressure gradient. This effect tends to diminish with fluids that have higher yield stress.

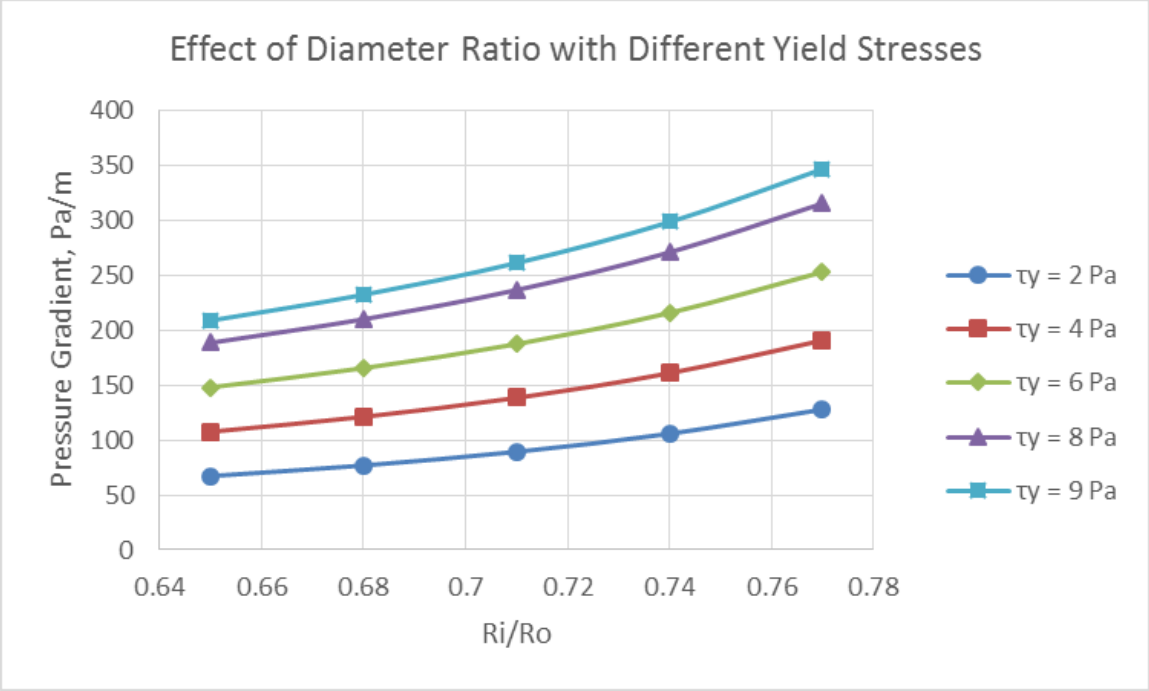

Figure 5-1. Effect of Diameter Ratio with Different Yield Stresses on Surge and Swab Pressure Gradient for YPL Fluid

5.2.2 Effect of Pipe Velocity

The effect of drillstring velocity on surge and swab pressures with different flow behavior indices is illustrated in Figure 5-2. It is seen that the higher the trip speed, higher the pressure change in the well. Moreover, pressure changes become less sensitive to trip speed as the fluid behaves more like shear thinning with decreasing flow behavior index.

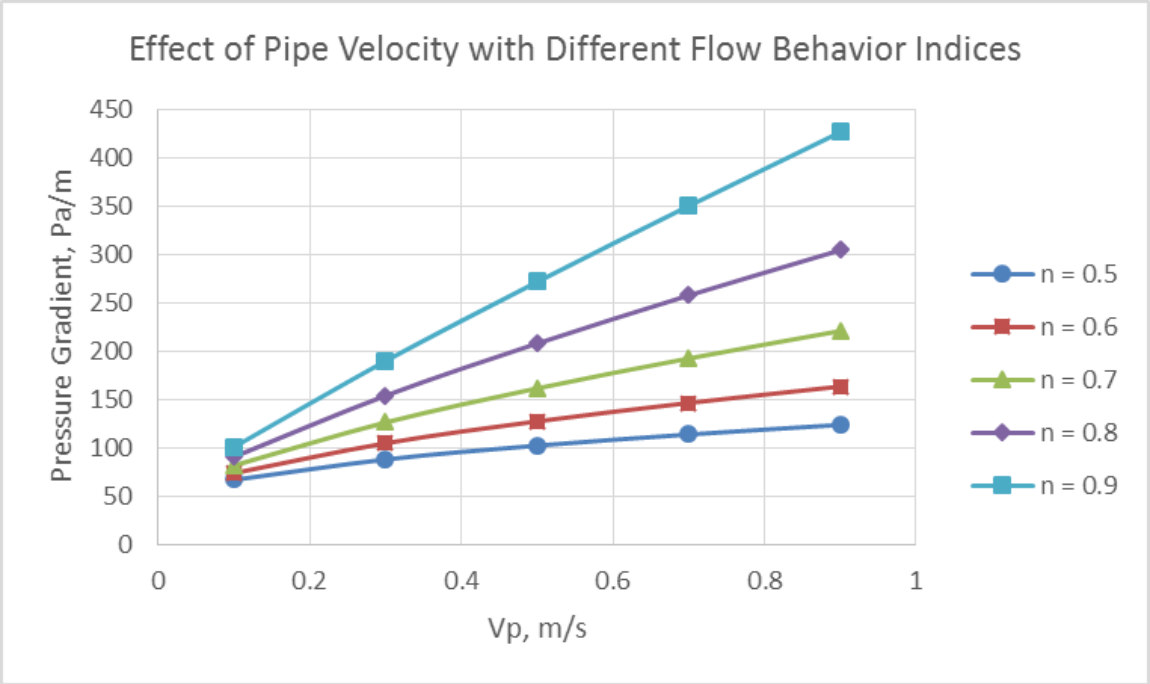

Figure 5-2. Effect of Pipe Velocity with Different Flow Behavior Indices on Surge and Swab Pressure Gradient for YPL Fluid

5.2.3 Effect of Yield Stress

Figure 5-3 shows the effect of yield stress of YPL drilling fluids on surge and swab pressure with different tripping speeds. At higher yield stress values, the pressure change in the hole becomes higher regardless of the magnitude of the trip velocity. On the other hand, increasing pipe velocity tends to increase the pressure change more, but with a decreasing rate.

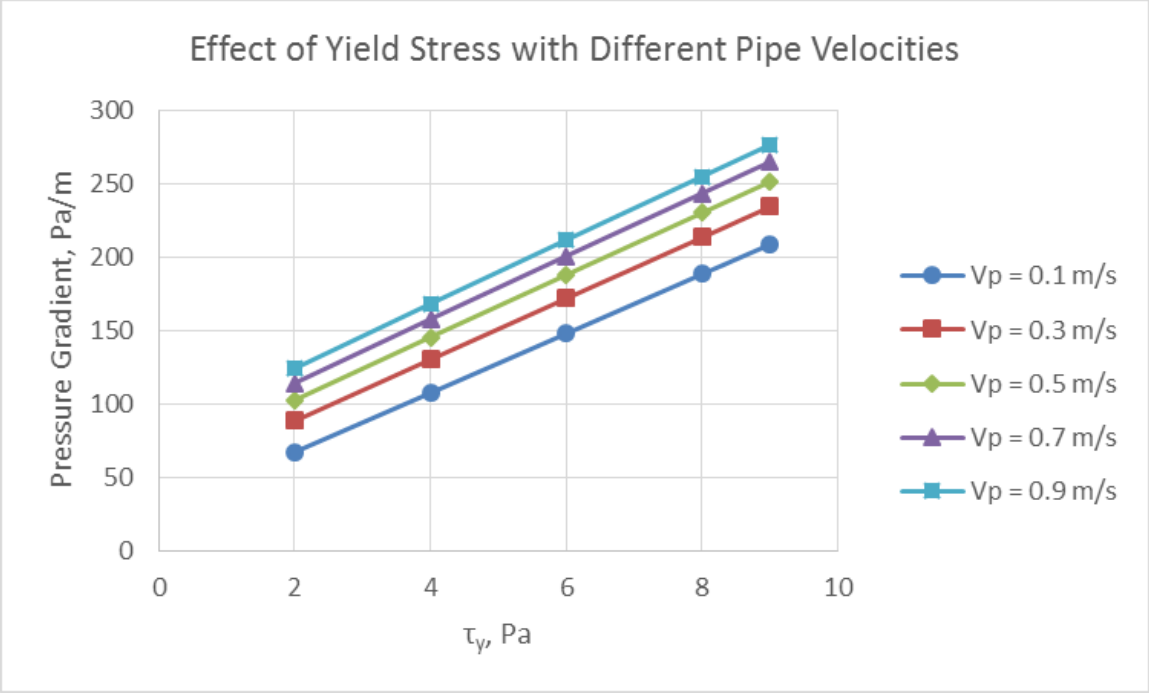

Figure 5-3. Effect of Yield Stress with Different Pipe Velocities on Surge and Swab Pressure Gradient for YPL Fluid

5.2.4 Effect of Flow Behavior Index

Increasing the flow behavior index means that the fluid is losing its shear-thinning ability. Therefore, it is easy to anticipate the direct proportionality between flow behavior index of drilling fluid with surge and swab pressure gradient as shown in Figure 5-4. Due to exponential nature of flow behavior index in Equation B-17, the rate of change of pressure losses with varying flow behavior index is also exponential. Furthermore, this effect is more apparently seen in narrow annuli as diameter ratio increases.

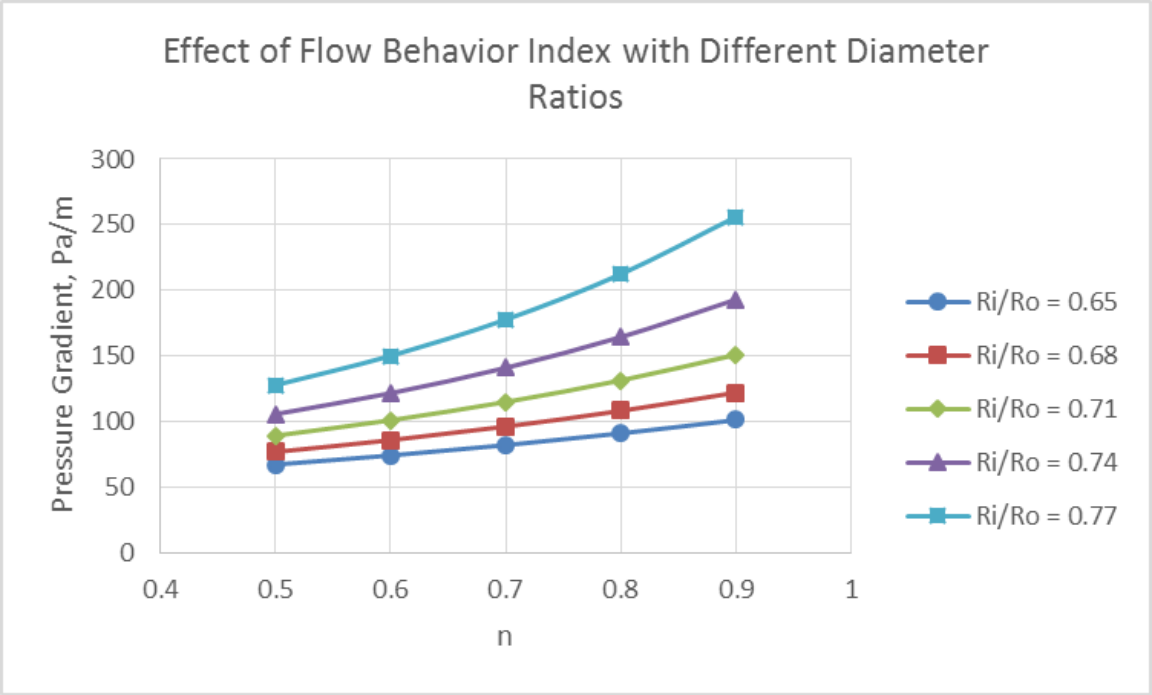

Figure 5-4. Effect of Flow Behavior Index with Different Diameter Ratios on Surge and Swab Pressure Gradient for YPL Fluid

CHAPTER 6

CONCLUSIONS AND RECOMMENDATIONS

6.1 Conclusions

After analyzing the sensitivity runs of surge and swab pressures, following conclusions can be reached in this study:

- Significant surge and swab pressures can occur while moving the drillstring.
- Surge and swab pressures are higher as the diameter ratio increases. Means, for narrow annuli the pressure is more pronounced compared to the swab and surge pressures at a wider annuli. Therefore, caution should be taken especially at the further sections of the wellbore where the casing and wellbore size decreases as the depth is increased.
- Increasing the yield of the fluid causes more pronounced surge and swab pressures. Therefore, a good optimization of yield stress of drilling fluid is necessary while trying to keep the hole clean.
- Decreasing the shear thinning ability of the fluid, i.e. increasing flow behavior index, causes the surge and swab pressure to be higher.
- An increase in the pipe velocity causes an increase in the rate of flow that is induced by the axial motion of inner pipe. Therefore, as anticipated, it increases the surge and swab pressure.
- Sensitivity analysis shows that diameter ratio and flow behavior index have significant effect on surge and swab pressure gradients, due to their exponential nature.

Overall, it is vital to practice drilling in a safe and optimized intervals of such parameters.

6.2 Recommendation for Future Studies

The following points are recommended for the future studies:

- Further work should be conducted to incorporate the effect of eccentricity and pipe rotation at surge and swab pressure of Yield Power Law fluids.
- Experimental works with Yield Power Law fluids are very limited in the literature, more experiments should be conducted with various fluids and geometries.
- The current study show the usefulness of CFD simulations to accurately capture the wellbore hydraulics challenges. CFD simulations should be further utilized to explain complex fluids and/or geometries, i.e. eccentric annuli, viscoplastic fluids, etc.

REFERENCES

ANSYS. (2013). Ansys Fluent 14.0 Tutorial Guide. *SAS IP, Inc*. doi:10.1016/0140-3664(87)90311-2

Beck, R. W., Nuss, W. F., & Dunn, T. H. (1947). The Flow Properties of Drilling Muds.

Bing, Z., Kaiji, Z., & Qiji, Y. (1995). Equations Help Calculate Surge and Swab Pressures in Inclined Wells. *Oil and Gas Journal*.

Bird, R. B., Stewart, W. E., & Lightfoot, E. N. (2002). *Transport Phenomena*. Retrieved from http://eu.wiley.com/WileyCDA/WileyTitle/productCd-0470115394.html

Bourgoyne Jr, A. T., Millheim, K. K., Chenevert, M. E., & Young Jr, F. . (1991). *Applied Drilling Engineering*.

Burkhardt, J. (1961). Wellbore Pressure Surges Produced by Pipe Movement. *Journal of Petroleum Technology*, *Volume 13*(Number 6), 595–605. doi:10.2118/1546-G

Cannon, G. E. (1934). Changes in Hydrostatic Pressure Due to Withdrawing Drill Pipe from the Hole. *API Drilling and Production Practices*, (April), 42–47.

Cardwell Jr., W. T. (1934). Pressure Changes in Drilling Wells caused by Pipe Movement. *API Drilling and Production Practices*, (June), 97–112.

Chin, W. C. (2011). Managed Pressure Drilling : Modeling , Strategy and Planning, (08121). Houston, TX: Stratamagnetic Software, LLC

Clark, E. H. (1955). Bottom-Hole Pressure Surges While Running Pipe. *The American Society of Mechanical Engineers*, (54-PET-22).

Crespo, F., & Ahmed, R. (2013). A simplified surge and swab pressure model for yield power law fluids. *Journal of Petroleum Science and Engineering*, *101*, 12–20. doi:10.1016/j.petrol.2012.10.001

Erge, O. (2013). *Effect of Free Drillstring Rotation on Frictional Pressure Losses* (Master's thesis, University of Tulsa)

Flumerfelt, R. W., Pierick, M. W., Cooper, S. L., & Bird, R. B. (1969). Generalized Plane Couette Flow of a Non-Newtonian Fluid. *Industrial & Engineering Chemistry Fundamentals*, *8*, 354–357. doi:10.1021/i160030a028

Fontenot, J. E., & Clark, R. . (1974). An Improved Method for Calculating Swab and Surge Pressures and Circulating Pressures in a Drilling Well. *SPE*, (4521), 451.

Forsythe, G. E., Malcolm, M. A., & Moler, C. B. (1977). *Computer Methods For Mathematical Computations*. Eaglewood Cliffs, NJ: Prentice Hall, Inc.

George S. Ormsby. (1954). Calculation and Control of Mud Pressures in Drilling and Completion Operations. In *Drilling and Production Practice* (p. 44).

Goins Jr, W. ., Weichert, J. ., Burba Jr, J. ., Dawson Jr, D. ., & Teplitz, A. . (1951). Down- the-hole Pressure Surges and Their Effect on Loss of Circulationt. In *API Drilling and Production Practices* (p. 125).

Haige, W., & Xisheng, L. (1996). Study on Steady Surge Pressure for Yield-Pseudoplastic Fluid in a Concentric Annulus. *Applied Mathematics and Mechanics*, *17*(1), 15–23.

Hussain, Q. E., & Sharif, M. A. R. (1997). Viscoplastic Fluid Flow in Irregular Eccentric Annuli Due to Axial Motion of the Inner Pipe. *The Canadian Journal of Chemical Engineering*, *75*, 1038–1045.

Lal, M. (1983). Surge and Swab Modeling for Dynamic Pressures and Safe Trip Velocities. *IADC/SPE Drilling Conference*, (11412), 427. doi:10.2118/11412-MS

Lin, S. H., & Hsu, C. C. (1980). Generalized Couette Flow of a Non-Newtonian Fluid in Annuli. *Industrial & Engineering Chemistry Fundamentals*, *19*(4), 421–424. doi:10.1021/i160076a017

Lubinski, A., Hsu, F. H., & Nolte, K. G. (1977). Transient Pressure Surges Due to Pipe Movement in an Oil Well. In *Revue de l'Inst. Franc. Du Pet.* (pp. 307–347).

MacSporran, W. C. (1982). Comments on: "Generalized Couette Flow of a Non-Newtonian Fluid in Annuli." *Ind. Eng. Chem. Fundam.*, *21*(1980), 98–99.

Malik, R., & Shenoy, U. V. (1991). Generalized Annular Couette Flow of a Power-Law Fluid. *American Chemical Society*, (8), 1950–1954.

Mitchell, R. F. (1988). Dynamic Surge/Swab Pressure Predictions. *SPE Drilling Engineering*, *3*(3), 325–333. doi:10.2118/16156-PA

Moore, P. L. (1986). *Drilling practices manual*. Tulsa, OK: Pennwell Publishing Company

R.S., R. (2000). New Formula of Surge Pressure for Determining Safe Trip Velocities. In *Proceedings of SPE Asia Pacific Oil and Gas Conference and Exhibition*. doi:10.2523/64480-MS

Rommetveit, R., Bjorkevoll, K., Gravdal, J. E., Goncalves, C., Lage, A., Campos, J., … Ohara, S. (2005). Ultradeepwater Hydraulics and Well-Control Tests With Extensive Instrumentation: Field Tests and Data Analysis. *SPE Drilling & Completion*, *20*(4), 251–257. doi:10.2118/84316-PA

Samuel, G., Sunthankar, A., McColpin, G., Bern, P., & Flynn, T. (2003). Field Validation of Transient Swab-Surge Response With Real-Time Downhole Pressure Data. *SPE Drilling & Completion*, *18*(4), 2001–2004. doi:10.2118/85109-PA

Samuel, R. (2010). Friction factors: What are they for torque, drag, vibration, bottom hole assembly and transient surge/swab analyses? *Journal of Petroleum Science and Engineering*, *73*(3-4), 258–266. doi:10.1016/j.petrol.2010.07.007

Schuh, F. J. (1964). Computer Makes Surge-Pressure Calculations Useful. *The Oil and Gas Journal*, 96.

Wagner, R. R., Halal, A. S., & Goodman, M. A. (1993). Surge Field Tests Highlight Dynamic Fluid Response. In *SPE/IADC Drilling Conference in Amsterdam* (pp. 883–892).

Wang, Y., & Chukwu, G. a. (1996). Unsteady Axial Laminar Couette Flow of Power-Law Fluids in a Concentric Annulus. *Industrial & Engineering Chemistry Research*, *35*(6), 2039–2047. Retrieved from <Go to ISI>://A1996UQ70500030

White, F. (2010). *Fluid Mechanics*. *McGraw-Hill,New York*. doi:10.1111/j.1549-8719.2009.00016.x.Mechanobiology

Wolski, A., Junqueira, S. L. M., & Negrão, C. O. R. (2014). A steady-state approach for evaluation of surge and swab pressures in flows with free surface boundary conditions. *Journal of Petroleum Science and Engineering*, *122*, 208–215. doi:10.1016/j.petrol.2014.07.011

Yang, L., & Chukwu, G. a. (1995). Couette Flow of Non-Newtonian Power-Law Fluids in Narrow Eccentric Annuli. *Industrial & Engineering Chemistry Research*, *34*, 936–942.

Zuo, W. (2005). *Introduction of Computational Fluid Dynamics*. Retrieved from http://www14.in.tum.de/konferenzen/Jass05/courses/2/Zuo/Zuo_paper.pdf

APPENDIX A

DERIVATION OF THE ANALYTICAL SOLUTION FOR SURGE AND SWAB PRESSURES OF NEWTONIAN FLUIDS IN CONCENTRIC ANNULI

We consider flow in annulus between two concentric cylinders, as illustrated in Figure 2-1, in which the inner cylinder moves in axial direction with a constant speed, while the outer cylinder stays stationary. The derivation includes following assumptions:

- Flow is steady state
- Gravitational force is neglected
- No slip at wellbore
- Flow is isothermal
- Flow is only in axial direction
- Fluid is incompressible
- Closed-ended pipe

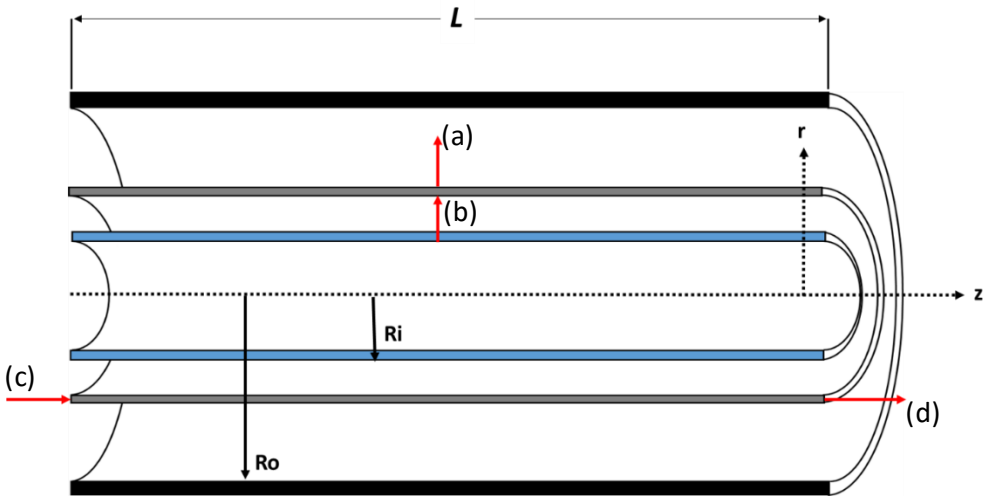

Figure A-1. Momentum Balance of a Thin Film between Inner Pipe and Annulus

(a) $\phi_{rz}|_{r+\Delta r} = flux\ of\ z-momentum\ out\ at\ r+\Delta r$

(b) $\phi_{rz}|_{r} = flux\ of\ z-momentum\ in\ at\ r$

(c) $\phi_{zz}|_{z=0} = flux\ of\ z-momentum\ in\ at\ z=0$

(d) $\phi_{zz}|_{z=L} = flux\ of\ z-momentum\ out\ at\ z=L$

Boundary conditions are as follows:

- at $r = \lambda R_o$, $\tau_{rz} = 0$
- at $r = R_o$, $v_z = 0$
- at $r = R_{cling}$, $v_z = 0$
- at $r = R_i$, $v_z = v_p$

Similar to the momentum influx examples in Chapter 2 of Bird et al. (2002), the momentum balance illustrated in Figure A-1:

$$2\pi rL\phi_{rz}|_{r} - 2\pi rL\phi_{rz}|_{r+\Delta r} + 2\pi\Delta r r\phi_{zz}|_{z=0} - 2\pi\Delta r r\phi_{zz}|_{z=L} - 2\pi\Delta rL\rho g = 0 \qquad \text{(A-1)}$$

Since gravitational force is neglected, the term $2\pi\Delta rL\rho g$ diminishes. Equation A-1 is divided by $2\pi\Delta rL$ and limit is taken as $\Delta r \to 0$, Equation A-1 becomes:

$$\lim_{\Delta r\to 0}\left(\frac{r\phi_{rz}|_{r+\Delta r} - r\phi_{rz}|_{r}}{\Delta r}\right) = \left(\frac{r\phi_{zz}|_{z=0} - r\phi_{zz}|_{z=L}}{\mathrm{L}}\right) \qquad \text{(A-2)}$$

The expression on the left side of the Equation A-2 is the first derivative of $r\phi_{rz}$ with respect to r. Therefore:

$$\frac{\partial(r\phi_{rz})}{\partial r} = \left(\frac{r\phi_{zz}|_{z=0} - r\phi_{zz}|_{z=L}}{\mathrm{L}}\right) \qquad \text{(A-3)}$$

Equation A-4 and A-5 are the momentum fluxes in the rz and rr directions:

$$\phi_{rz} = \tau_{rz} + \rho v_r v_z \tag{A-4}$$

$$\phi_{zz} = P + \tau_{zz} + \rho v_z v_z \tag{A-5}$$

Since the flow is only in axial direction, the velocity term in the r direction is zero, $\rho v_r v_z$ term drops. Also, $v_z = v_z(r)$. So, $\rho v_z v_z$ and τ_{zz} become same at both ends of the tube. Therefore, Equation A-3 becomes:

$$\frac{d(r\tau_{rz})}{dr} = \left(\frac{P_0 - P_L}{L}\right) r = \left(-\frac{\mathrm{dP}}{\mathrm{d}l} r\right) \tag{A-6}$$

Integration of Equation A-6 gives:

$$\tau_{rz} = \left(-\frac{\mathrm{dP}}{\mathrm{d}l}\frac{r}{2}\right) + \frac{C_1}{r} \tag{A-7}$$

Applying boundary condition; at $r = \lambda R_o$, and $\tau_{rz} = 0$ gives:

$$0 = \left(-\frac{\mathrm{dP}}{\mathrm{d}l}\frac{\lambda R_o}{2}\right) + \frac{C_1}{\lambda R_o} \qquad \rightarrow \qquad C_1 = \frac{\mathrm{dP}}{\mathrm{d}l}\frac{\lambda^2 {R_o}^2}{2} \tag{A-8}$$

Inserting C_1 into Equation A-7:

$$\tau_{rz} = \left(-\frac{\mathrm{dP}}{\mathrm{d}l}\frac{r}{2}\right) + \frac{\frac{\mathrm{dP}}{\mathrm{d}l}\frac{\lambda^2 {R_o}^2}{2}}{r} \tag{A-9}$$

τ_{rz} now becomes:

$$\tau_{rz} = \left(-\frac{\mathrm{dP}}{\mathrm{d}l}\frac{R_o}{2}\right)\left(\frac{r}{R_o} - \lambda^2\frac{R_o}{r}\right) \tag{A-10}$$

Below is the Newton`s Law of viscosity:

$$\tau_{rz} = \left(-\mu \frac{dv_z}{dr}\right) \tag{A-11}$$

Combining Equation A-10 and Equation A-11 gives:

$$\left(-\frac{\mathrm{dP}}{\mathrm{d}l}\frac{R_o}{2}\right)\left(\frac{r}{R_o} - \lambda^2 \frac{R_o}{r}\right) = \left(-\mu \frac{dv_z}{dr}\right) \tag{A-12}$$

Equation A-12 can be rewritten as:

$$\left[\frac{\left(\frac{\mathrm{dP}}{\mathrm{d}l}\frac{R_o}{2}\right)\left(\frac{r}{R_o} - \lambda^2 \frac{R_o}{r}\right)}{\mu}\right] dr = dv_z \tag{A-13}$$

Integrating Equation A-13:

$$\int \left[\frac{\left(\frac{\mathrm{dP}}{\mathrm{d}l}\frac{r}{2} - \frac{\mathrm{dP}}{\mathrm{d}l}\frac{{R_o}^2\lambda^2}{2r}\right)}{\mu}\right] dr = \int dv_z \tag{A-14}$$

$$\frac{\mathrm{dP}}{\mathrm{d}l}\frac{r^2}{4\mu} - \frac{\mathrm{dP}}{\mathrm{d}l}\frac{{R_o}^2\lambda^2}{2\mu} ln(r) + C_2 = v_z \tag{A-15}$$

Applying boundary condition; at $r = R_i$, $v_z = v_p$ to Equation A-15 gives:

$$\frac{\mathrm{dP}}{\mathrm{d}l}\frac{{R_i}^2}{4\mu} - \frac{\mathrm{dP}}{\mathrm{d}l}\frac{{R_o}^2\lambda^2}{2\mu} ln(R_i) + C_2 = v_p \tag{A-16}$$

C_2 can be written as:

$$C_2 = v_p - \frac{\mathrm{dP}}{\mathrm{d}l}\frac{{R_i}^2}{4\mu} + \frac{\mathrm{dP}}{\mathrm{d}l}\frac{{R_o}^2\lambda^2}{2\mu}ln(R_i) \tag{A-17}$$

Substituting C_2 back into Equation A-15:

$$\frac{\mathrm{dP}}{\mathrm{d}l}\frac{r^2}{4\mu} - \frac{\mathrm{dP}}{\mathrm{d}l}\frac{{R_o}^2\lambda^2}{2\mu}ln(r) + v_p - \frac{\mathrm{dP}}{\mathrm{d}l}\frac{{R_i}^2}{4\mu} + \frac{\mathrm{dP}}{\mathrm{d}l}\frac{{R_o}^2\lambda^2}{2\mu}ln(R_i) = v_z \tag{A-18}$$

Applying boundary condition; at $r = R_o$, $v_z = 0$ to Equation A-18 gives:

$$\frac{\mathrm{dP}}{\mathrm{d}l}\frac{{R_o}^2}{4\mu} - \frac{\mathrm{dP}}{\mathrm{d}l}\frac{{R_o}^2\lambda^2}{2\mu}ln(R_o) + v_p - \frac{\mathrm{dP}}{\mathrm{d}l}\frac{{R_i}^2}{4\mu} + \frac{\mathrm{dP}}{\mathrm{d}l}\frac{{R_o}^2\lambda^2}{2\mu}ln(R_i) = 0 \tag{A-19}$$

Equation A-19 can be rewritten as:

$$-\frac{\mathrm{dP}}{\mathrm{d}l}\frac{{R_o}^2\lambda^2}{2\mu}ln(R_o) + \frac{\mathrm{dP}}{\mathrm{d}l}\frac{{R_o}^2\lambda^2}{2\mu}ln(R_i) = -\frac{\mathrm{dP}}{\mathrm{d}l}\frac{\left({R_o}^2 - {R_i}^2\right)}{4\mu} - v_p \tag{A-20}$$

Simplification of Equation A-20 gives:

$$-\frac{\mathrm{dP}}{\mathrm{d}l}\frac{{R_o}^2\lambda^2}{2\mu}ln\left(\frac{R_o}{R_i}\right) = -\frac{\mathrm{dP}}{\mathrm{d}l}\frac{\left({R_o}^2 - {R_i}^2\right)}{4\mu} - v_p \tag{A-21}$$

$$-\frac{\mathrm{dP}}{\mathrm{d}l}\frac{{R_o}^2\lambda^2}{2\mu} = -\frac{\frac{\mathrm{dP}}{\mathrm{d}l}\frac{\left({R_o}^2 - {R_i}^2\right)}{4\mu} + v_p}{ln\left(\frac{R_o}{R_i}\right)} \tag{A-22}$$

Equation A-18 can be rewritten as:

$$\frac{\mathrm{dP}}{\mathrm{d}l}\frac{r^2}{4\mu} - \frac{\mathrm{dP}}{\mathrm{d}l}\frac{{R_o}^2\lambda^2}{2\mu}ln\left(\frac{r}{R_i}\right) + v_p - \frac{\mathrm{dP}}{\mathrm{d}l}\frac{{R_i}^2}{4\mu} = v_z \tag{A-23}$$

Combining Equation A-22 and Equation A-23 gives the final form of the exact solution for velocity at any position 'r' as:

$$v_z = \frac{\mathrm{dP}}{\mathrm{d}l}\frac{\left(r^2 - {R_i}^2\right)}{4\mu} - \left[\frac{\mathrm{dP}}{\mathrm{d}l}\frac{\left({R_o}^2 - {R_i}^2\right)}{4\mu} + v_p\right]\frac{ln\left(\frac{r}{R_i}\right)}{ln\left(\frac{R_o}{R_i}\right)} + v_p \qquad \text{(A-24)}$$

APPENDIX B

DERIVATION OF THE NUMERICAL SOLUTION FOR SURGE AND SWAB PRESSURES OF NEWTONIAN FLUIDS IN CONCENTRIC ANNULI

Assumptions made as derivation of numerical analysis:

- Flow is steady state
- Flow is only in axial direction
- Flow is axisymmetric
- Flow is fully developed
- Gravitational force is neglected
- Fluid is incompressible
- Closed-ended pipe
- No slip at wellbore
- Flow is isothermal

Numerical model derivation for implicit finite difference scheme for laminar surge and swab of fluids in concentric annulus.

Continuity Equation in cylindrical coordinates:

Axial flow only | Fully developed | Steady state flow | Axial flow only

$$\left(\frac{\partial \rho}{\partial t}+\frac{1}{r}\frac{\partial(\rho r v_r)}{\partial r}+\frac{1}{r}\frac{\partial(\rho v_\theta)}{\partial \theta}+\frac{\partial(\rho v_z)}{\partial z}\right)=0 \tag{B-1}$$

Satisfies the condition.

Equation of motion in z direction in cylindrical coordinates:

$$\rho\left(\frac{\partial v_z}{\partial t}+v_r\frac{\partial v_z}{\partial r}+\frac{v_\theta}{r}\frac{\partial v_z}{\partial \theta}+v_z\frac{\partial v_z}{\partial z}\right) = -\frac{\partial p}{\partial z}-\left[\frac{1}{r}\frac{\partial}{\partial r}(r\tau_{rz})+\frac{1}{r}\frac{\partial}{\partial \theta}\tau_{\theta z}+\frac{\partial}{\partial z}\tau_{zz}\right]+\quad \rho g_z \tag{B-2}$$

Where, the stress tensors for cylindrical coordinates are:

$$\tau_{zr}=\tau_{rz}=-\mu\left[\frac{\partial v_r}{\partial z}+\frac{\partial v_z}{\partial r}\right] \tag{B-3}$$

$$\tau_{z\theta}=\tau_{\theta z}=-\mu\left[\frac{1}{r}\frac{\partial v_z}{\partial \theta}+\frac{\partial v_\theta}{\partial z}\right] \tag{B-4}$$

$$\tau_{zz}=-\mu\left[2\frac{\partial v_z}{\partial z}\right]+\left(\frac{2}{3}\mu-\kappa\right)(\nabla\cdot V) \tag{B-5}$$

The term contains $(\nabla\cdot V)$ will be omitted, since the fluid is assumed to be incompressible (Bird et al., 2002).

Left hand side of the Equation B-2 diminishes as:

Steady state flow | Axisymmetric flow

$$\rho\left(\frac{\partial v_z}{\partial t}+v_r\frac{\partial v_z}{\partial r}+\frac{v_\theta}{r}\frac{\partial v_z}{\partial \theta}+v_z\frac{\partial v_z}{\partial z}\right) \tag{B-6}$$

Axial flow only | Fully developed flow

Right hand side of the Equation B-2 can be rewritten as:

Axisymmetric flow

Axial flow only | Axial flow only

$$-\frac{\partial p}{\partial z}-\left[-\frac{1}{r}\frac{\partial}{\partial r}\left(r\mu\left[\frac{\partial v_r}{\partial z}+\frac{\partial v_z}{\partial r}\right]\right)-\frac{1}{r}\frac{\partial}{\partial \theta}\left(\mu\left[\frac{1}{r}\frac{\partial v_z}{\partial \theta}+\frac{\partial v_\theta}{\partial z}\right]\right)\right.$$

$$\left.-\frac{\partial}{\partial z}\left(\mu\left[2\frac{\partial v_z}{\partial z}\right]+\left(\frac{2}{3}\mu-\kappa\right)(\nabla\cdot V)\right)\right]+\rho g_z \tag{B-7}$$

Fully developed flow | No gravitational force

Incompressible fluid

$$\frac{\partial p}{\partial z}=\frac{1}{r}\frac{\partial}{\partial r}\left(\mu r\frac{\partial v_z}{\partial r}\right) \tag{B-8}$$

Which can be rewritten as:

$$\frac{\partial p}{\partial z}=\frac{1}{r}\left(\mu\frac{\partial v_z}{\partial r}+\mu r\frac{\partial^2(v_z)}{\partial r^2}\right) \tag{B-9}$$

In another form, the Equation B-9 can be written as:

$$\frac{\partial p}{\partial z} = \left[\frac{\partial}{\partial r}\left(\mu \frac{\partial (v_z)}{\partial r}\right)\right] + \left[\frac{1}{r}\mu \frac{\partial (v_z)}{\partial r}\right] \tag{B-10}$$

Discretizing Equation B-10:

$$\frac{\partial p}{\partial z} = \frac{\left[\left(\mu \frac{\partial (v_z)}{\partial r}\right)_{i+1/2} - \left(\mu \frac{\partial (v_z)}{\partial r}\right)_{i-1/2}\right] + \frac{1}{r}\mu \frac{v_{i+1} - v_{i-1}}{2}}{\Delta r} \tag{B-11}$$

where $(\mu)_{i+1/2}$ can be written as $\frac{1}{2}(\mu_{i+1} + \mu_i)$

$$\frac{\partial p}{\partial z}\Delta r = \left(\frac{1}{2}(\mu_{i+1} + \mu_i)\left(\frac{\partial (v_z)}{\partial r}\right)_{i+1/2} - \frac{1}{2}(\mu_i + \mu_{i-1})\left(\frac{\partial (v_z)}{\partial r}\right)_{i-1/2}\right) + \frac{1}{r}\mu \frac{v_{i+1} - v_{i-1}}{2} \tag{B-12}$$

$$\frac{\partial p}{\partial z}\Delta r = \frac{1}{2}\left((\mu_{i+1} + \mu_i)\frac{v_{i+1} - v_i}{\Delta r} - (\mu_i + \mu_{i-1})\frac{v_i - v_{i-1}}{\Delta r}\right) + \mu \frac{v_{i+1} - v_{i-1}}{2r} \tag{B-13}$$

Equation B-13 can be rewritten as:

$$\frac{\partial p}{\partial z} 2\Delta r^2 = (\mu_{i+1} + \mu_i)(v_{i+1}) - (\mu_{i+1} + 2\mu_i + \mu_{i-1})(v_i) + (\mu_i + \mu_{i-1})(v_{i-1}) + \mu_i \Delta r \frac{v_{i+1} - v_{i-1}}{r} \tag{B-14}$$

Final form of numerical solution becomes:

$$\frac{\partial p}{\partial z} 2\Delta r^2 = \left(\left({\mu_{i+1}}^k + {\mu_i}^k + {\mu_i}^k \frac{\Delta r}{r} \right) ({v_{i+1}}^{k+1}) \right.$$

$$- ({\mu_{i+1}}^k + 2{\mu_i}^k + {\mu_{i-1}}^k)({v_i}^{k+1}) \qquad \text{(B-15)}$$

$$\left. + \left({\mu_i}^k + {\mu_{i-1}}^k - {\mu_i}^k \frac{\Delta r}{r} \right) ({v_{i-1}}^{k+1}) \right)$$

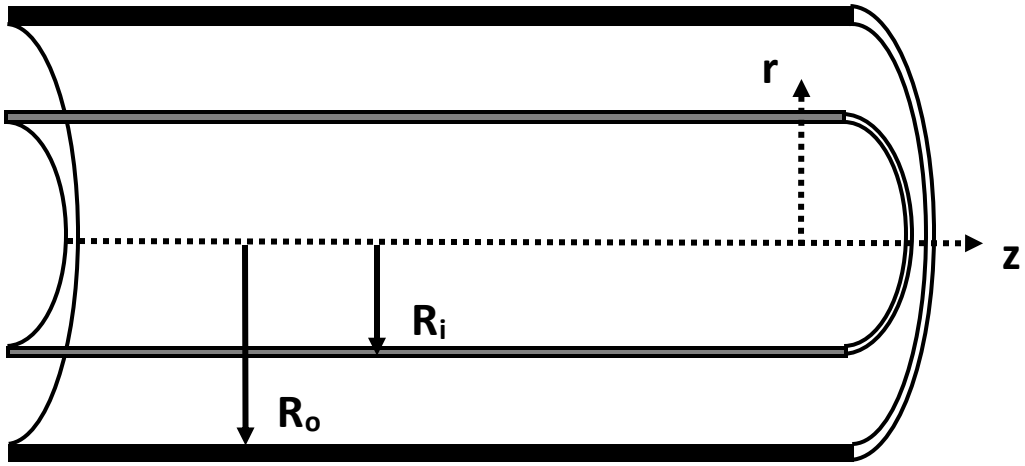

Figure B-1. Cross-section of Annulus

Typical boundary conditions for estimating surge and swab pressures in concentric annulus would be:

- at $r = R_o$, $v_z = 0$
- at $r = R_i$, $v_z = v_p$

An apparent viscosity needs to be defined since the fluid is non-Newtonian (Erge, 2013). Viscosity terms in Equation B-15 will be replaced with μ_{app}.

$$\mu_{app} = \frac{\tau}{\gamma} \qquad \text{(B-16)}$$

In which YPL defines τ as:

$$\tau = \tau_0 + K\gamma^n \qquad \text{(B-17)}$$

Apparent viscosity function for YPL fluids can be defined as:

$$\mu_{app} = \frac{\tau_0}{\gamma} + K\gamma^{n-1} \tag{B-18}$$

Where shear rate function given as:

$$\gamma = \frac{\partial v_r}{\partial z} \tag{B-19}$$

APPENDIX C

VELOCITY PROFILE COMPARISON TABLES

Comparison of velocity profile in z-direction at annulus while surge or swab took place are presented using graphs in Chapter 4 of this thesis. The comparison is made among analytical solution results obtained from Chin (2011), numerical and analytical solution derived in this study, and CFD Fluent analysis results. Input parameters using the comparison study are listed in below Table C-1.

Table C-1. Inputs of Velocity Profile Comparison

Input Parameters - Newtonian	
μ	0.001 Pa.s
R_o	0.0254 m
R_i	0.016764 m
V_p	0.01 m/s
dP/dl	0.67272 Pa/m

Numerical results of annular velocity profile comparison study for swab condition of Newtonian fluids are tabulated in Table C-2.

Table C-2. Velocity Profile Comparison Table

	Velocity Profile with Corresponding Radius (m/s)			
r (m)	Chin – Analytical	This Study – Analytical	This Study – Numerical	CFD – Fluent
0.01676	0.01000	0.01000	0.01000	0.00998
0.01685	0.00960	0.00960	0.00960	0.00961
0.01694	0.00921	0.00921	0.00921	0.00925
0.01703	0.00883	0.00883	0.00883	0.00888
0.01711	0.00846	0.00846	0.00846	0.00852
0.01720	0.00809	0.00809	0.00809	0.00815
0.01729	0.00773	0.00773	0.00773	0.00779
0.01737	0.00737	0.00737	0.00737	0.00742
0.01746	0.00702	0.00702	0.00702	0.00705
0.01755	0.00668	0.00668	0.00668	0.00669
0.01764	0.00635	0.00635	0.00635	0.00636
0.01772	0.00602	0.00602	0.00602	0.00605
0.01781	0.00570	0.00570	0.00570	0.00573
0.01790	0.00539	0.00539	0.00539	0.00542
0.01799	0.00508	0.00508	0.00508	0.00511
0.01807	0.00478	0.00478	0.00478	0.00480
0.01816	0.00449	0.00449	0.00449	0.00449
0.01825	0.00420	0.00420	0.00420	0.00417
0.01833	0.00392	0.00392	0.00392	0.00386
0.01842	0.00364	0.00364	0.00364	0.00355
0.01851	0.00338	0.00338	0.00338	0.00326
0.01860	0.00311	0.00311	0.00311	0.00302
0.01868	0.00286	0.00286	0.00286	0.00279
0.01877	0.00261	0.00261	0.00261	0.00256
0.01886	0.00237	0.00237	0.00237	0.00232
0.01894	0.00213	0.00213	0.00213	0.00209
0.01903	0.00190	0.00190	0.00190	0.00185
0.01912	0.00167	0.00167	0.00167	0.00162
0.01921	0.00146	0.00146	0.00146	0.00139
0.01929	0.00124	0.00124	0.00124	0.00115
0.01938	0.00104	0.00104	0.00104	0.00092
0.01947	0.00084	0.00084	0.00084	0.00072
0.01956	0.00064	0.00064	0.00064	0.00056
0.01964	0.00046	0.00046	0.00046	0.00040
0.01973	0.00027	0.00027	0.00027	0.00024
0.01982	0.00010	0.00010	0.00010	0.00008
0.01990	-0.00007	-0.00007	-0.00007	-0.00008
0.01999	-0.00024	-0.00024	-0.00024	-0.00024

Table C-2 (continued)

0.02008	-0.00040	-0.00040	-0.00040	-0.00039
0.02017	-0.00055	-0.00055	-0.00055	-0.00055
0.02025	-0.00070	-0.00070	-0.00070	-0.00071
0.02034	-0.00084	-0.00084	-0.00084	-0.00087
0.02043	-0.00097	-0.00097	-0.00097	-0.00103
0.02051	-0.00110	-0.00110	-0.00110	-0.00112
0.02060	-0.00123	-0.00123	-0.00123	-0.00122
0.02069	-0.00134	-0.00134	-0.00134	-0.00132
0.02078	-0.00146	-0.00146	-0.00146	-0.00142
0.02086	-0.00157	-0.00157	-0.00157	-0.00151
0.02095	-0.00167	-0.00167	-0.00167	-0.00161
0.02104	-0.00176	-0.00176	-0.00176	-0.00171
0.02113	-0.00185	-0.00185	-0.00185	-0.00181
0.02121	-0.00194	-0.00194	-0.00194	-0.00190
0.02130	-0.00202	-0.00202	-0.00202	-0.00200
0.02139	-0.00209	-0.00209	-0.00209	-0.00210
0.02147	-0.00216	-0.00216	-0.00216	-0.00216
0.02156	-0.00223	-0.00223	-0.00223	-0.00220
0.02165	-0.00228	-0.00228	-0.00228	-0.00224
0.02174	-0.00234	-0.00234	-0.00234	-0.00228
0.02182	-0.00239	-0.00239	-0.00239	-0.00232
0.02191	-0.00243	-0.00243	-0.00243	-0.00236
0.02200	-0.00246	-0.00246	-0.00246	-0.00240
0.02209	-0.00250	-0.00250	-0.00250	-0.00243
0.02217	-0.00252	-0.00252	-0.00252	-0.00247
0.02226	-0.00254	-0.00254	-0.00254	-0.00251
0.02235	-0.00256	-0.00256	-0.00256	-0.00255
0.02243	-0.00257	-0.00257	-0.00257	-0.00257
0.02252	-0.00258	-0.00258	-0.00258	-0.00255
0.02261	-0.00258	-0.00258	-0.00258	-0.00254
0.02270	-0.00257	-0.00257	-0.00257	-0.00252
0.02278	-0.00256	-0.00256	-0.00256	-0.00250
0.02287	-0.00255	-0.00255	-0.00255	-0.00248
0.02296	-0.00253	-0.00253	-0.00253	-0.00246
0.02304	-0.00251	-0.00251	-0.00251	-0.00244
0.02313	-0.00248	-0.00248	-0.00248	-0.00242
0.02322	-0.00244	-0.00244	-0.00244	-0.00240
0.02331	-0.00240	-0.00240	-0.00240	-0.00238
0.02339	-0.00236	-0.00236	-0.00236	-0.00236
0.02348	-0.00231	-0.00231	-0.00231	-0.00229

Table C-2 (continued)

0.02357	-0.00225	-0.00225	-0.00225	-0.00221
0.02366	-0.00219	-0.00219	-0.00219	-0.00214
0.02374	-0.00213	-0.00213	-0.00213	-0.00206
0.02383	-0.00206	-0.00206	-0.00206	-0.00199
0.02392	-0.00199	-0.00199	-0.00199	-0.00191
0.02400	-0.00191	-0.00191	-0.00191	-0.00184
0.02409	-0.00182	-0.00182	-0.00182	-0.00176
0.02418	-0.00173	-0.00173	-0.00173	-0.00169
0.02427	-0.00164	-0.00164	-0.00164	-0.00161
0.02435	-0.00154	-0.00154	-0.00154	-0.00154
0.02444	-0.00144	-0.00144	-0.00144	-0.00143
0.02453	-0.00133	-0.00133	-0.00133	-0.00130
0.02461	-0.00122	-0.00122	-0.00122	-0.00117
0.02470	-0.00110	-0.00110	-0.00110	-0.00104
0.02479	-0.00098	-0.00098	-0.00098	-0.00091
0.02488	-0.00086	-0.00086	-0.00086	-0.00078
0.02496	-0.00072	-0.00072	-0.00072	-0.00065
0.02505	-0.00059	-0.00059	-0.00059	-0.00052
0.02514	-0.00045	-0.00045	-0.00045	-0.00039
0.02523	-0.00030	-0.00030	-0.00030	-0.00026
0.02531	-0.00015	-0.00015	-0.00015	-0.00013
0.02540	0.00000	0.00000	0.00000	0.00000

Dimensionless velocity profile comparison is listed in Table C-3. Note that definitions of dimensionless velocity and dimensionless radius are presented in Chapter 4.

Table C-3. Dimensionless Velocity Profile Comparison Table

	Dimensionless Velocity Profile with Corresponding Dimensionless Radius			
Dimensionless r	Chin (2011)	This Study – Analytical	This Study – Numerical	CFD Fluent
0.00000	1.00000	1.00000	1.00000	0.99767
0.01010	0.96033	0.96033	0.96033	0.96116
0.02020	0.92138	0.92138	0.92138	0.92464
0.03030	0.88314	0.88314	0.88314	0.88812
0.04040	0.84561	0.84561	0.84561	0.85160

Table C-3 (continued)

0.05050	0.80878	0.80878	0.80878	0.81507
0.06061	0.77264	0.77264	0.77264	0.77854
0.07071	0.73720	0.73720	0.73720	0.74200
0.08081	0.70244	0.70244	0.70244	0.70546
0.09091	0.66837	0.66837	0.66837	0.66892
0.10101	0.63498	0.63498	0.63498	0.63578
0.11111	0.60227	0.60227	0.60226	0.60457
0.12121	0.57022	0.57022	0.57022	0.57336
0.13131	0.53884	0.53884	0.53884	0.54217
0.14141	0.50813	0.50813	0.50813	0.51099
0.15151	0.47807	0.47807	0.47807	0.47981
0.16161	0.44867	0.44867	0.44867	0.44865
0.17172	0.41993	0.41993	0.41992	0.41749
0.18182	0.39183	0.39183	0.39182	0.38634
0.19192	0.36437	0.36437	0.36436	0.35521
0.20202	0.33755	0.33755	0.33755	0.32582
0.21212	0.31137	0.31137	0.31137	0.30242
0.22222	0.28583	0.28583	0.28582	0.27901
0.23232	0.26091	0.26091	0.26091	0.25561
0.24242	0.23662	0.23662	0.23662	0.23221
0.25252	0.21295	0.21295	0.21295	0.20880
0.26262	0.18991	0.18991	0.18990	0.18540
0.27272	0.16747	0.16747	0.16747	0.16200
0.28283	0.14566	0.14566	0.14565	0.13860
0.29293	0.12445	0.12445	0.12444	0.11520
0.30303	0.10384	0.10384	0.10384	0.09179
0.31313	0.08384	0.08384	0.08384	0.07214
0.32323	0.06444	0.06444	0.06444	0.05616
0.33333	0.04564	0.04564	0.04564	0.04020
0.34343	0.02743	0.02743	0.02743	0.02425
0.35353	0.00982	0.00982	0.00981	0.00830
0.36363	-0.00721	-0.00721	-0.00722	-0.00764
0.37373	-0.02366	-0.02366	-0.02366	-0.02357
0.38383	-0.03952	-0.03952	-0.03952	-0.03949
0.39394	-0.05480	-0.05480	-0.05480	-0.05540
0.40404	-0.06950	-0.06950	-0.06951	-0.07130
0.41414	-0.08363	-0.08363	-0.08364	-0.08720
0.42424	-0.09719	-0.09719	-0.09720	-0.10265
0.43434	-0.11019	-0.11019	-0.11019	-0.11241
0.44444	-0.12261	-0.12261	-0.12262	-0.12217

Table C-3 (continued)

0.45454	-0.13447	-0.13447	-0.13448	-0.13193
0.46464	-0.14577	-0.14577	-0.14578	-0.14169
0.47474	-0.15652	-0.15652	-0.15652	-0.15144
0.48484	-0.16670	-0.16670	-0.16671	-0.16120
0.49494	-0.17634	-0.17634	-0.17634	-0.17096
0.50505	-0.18542	-0.18542	-0.18543	-0.18071
0.51515	-0.19396	-0.19396	-0.19396	-0.19047
0.52525	-0.20195	-0.20195	-0.20195	-0.20023
0.53535	-0.20939	-0.20939	-0.20940	-0.20998
0.54545	-0.21630	-0.21630	-0.21630	-0.21628
0.55555	-0.22266	-0.22266	-0.22267	-0.22016
0.56565	-0.22849	-0.22849	-0.22850	-0.22403
0.57575	-0.23379	-0.23379	-0.23379	-0.22791
0.58585	-0.23855	-0.23855	-0.23855	-0.23179
0.59595	-0.24278	-0.24278	-0.24279	-0.23566
0.60605	-0.24649	-0.24649	-0.24649	-0.23954
0.61616	-0.24967	-0.24967	-0.24967	-0.24341
0.62626	-0.25233	-0.25233	-0.25233	-0.24729
0.63636	-0.25446	-0.25446	-0.25446	-0.25116
0.64646	-0.25608	-0.25608	-0.25608	-0.25504
0.65656	-0.25718	-0.25718	-0.25717	-0.25737
0.66666	-0.25776	-0.25776	-0.25776	-0.25546
0.67676	-0.25783	-0.25783	-0.25783	-0.25355
0.68686	-0.25739	-0.25739	-0.25739	-0.25163
0.69696	-0.25644	-0.25644	-0.25644	-0.24972
0.70706	-0.25498	-0.25498	-0.25498	-0.24781
0.71716	-0.25302	-0.25302	-0.25302	-0.24590
0.72727	-0.25055	-0.25055	-0.25055	-0.24398
0.73737	-0.24758	-0.24758	-0.24758	-0.24207
0.74747	-0.24412	-0.24412	-0.24411	-0.24016
0.75757	-0.24015	-0.24015	-0.24015	-0.23825
0.76767	-0.23569	-0.23569	-0.23568	-0.23633
0.77777	-0.23073	-0.23073	-0.23073	-0.22901
0.78787	-0.22528	-0.22528	-0.22528	-0.22148
0.79797	-0.21935	-0.21935	-0.21934	-0.21395
0.80807	-0.21292	-0.21292	-0.21291	-0.20643
0.81817	-0.20600	-0.20600	-0.20599	-0.19890
0.82827	-0.19860	-0.19860	-0.19859	-0.19137
0.83837	-0.19071	-0.19071	-0.19071	-0.18385
0.84848	-0.18235	-0.18235	-0.18234	-0.17632

Table C-3 (continued)

0.85858	-0.17350	-0.17350	-0.17349	-0.16879
0.86868	-0.16417	-0.16417	-0.16416	-0.16127
0.87878	-0.15436	-0.15436	-0.15435	-0.15374
0.88888	-0.14408	-0.14408	-0.14407	-0.14342
0.89898	-0.13333	-0.13333	-0.13332	-0.13033
0.90908	-0.12210	-0.12210	-0.12209	-0.11725
0.91918	-0.11040	-0.11040	-0.11039	-0.10416
0.92928	-0.09823	-0.09823	-0.09822	-0.09108
0.93938	-0.08559	-0.08559	-0.08558	-0.07799
0.94948	-0.07249	-0.07249	-0.07248	-0.06490
0.95959	-0.05892	-0.05892	-0.05890	-0.05182
0.96969	-0.04489	-0.04489	-0.04487	-0.03873
0.97979	-0.03039	-0.03039	-0.03037	-0.02565
0.98989	-0.01543	-0.01543	-0.01542	-0.01256
1.00000	0.00000	0.00000	0.00000	0.00000

Table C-4 shows the velocity values with corresponding radius for grid independence analysis.

Table C-4. Velocity Profile Comparison Table for Grid Independence Study

	Velocity Profile with Corresponding Radius (m/s)					
r (m)	This Study – Analytical	Mesh #1	Mesh #2	Mesh #3	Mesh #4	Mesh #5
0.01676	0.01000	0.00995	0.00983	0.00991	0.00998	0.00998
0.01685	0.00960	0.00973	0.00955	0.00957	0.00961	0.00956
0.01694	0.00921	0.00950	0.00927	0.00923	0.00925	0.00914
0.01703	0.00883	0.00927	0.00898	0.00889	0.00888	0.00872
0.01711	0.00846	0.00904	0.00870	0.00854	0.00852	0.00831
0.01720	0.00809	0.00881	0.00842	0.00820	0.00815	0.00789
0.01729	0.00773	0.00859	0.00814	0.00786	0.00779	0.00748
0.01737	0.00737	0.00836	0.00786	0.00752	0.00742	0.00706
0.01746	0.00702	0.00813	0.00757	0.00718	0.00705	0.00665
0.01755	0.00668	0.00788	0.00729	0.00684	0.00669	0.00624
0.01764	0.00635	0.00764	0.00701	0.00650	0.00636	0.00590
0.01772	0.00602	0.00739	0.00673	0.00616	0.00605	0.00563
0.01781	0.00570	0.00715	0.00645	0.00582	0.00573	0.00536
0.01790	0.00539	0.00691	0.00616	0.00549	0.00542	0.00510

Table C-4 (continued)

0.01799	0.00508	0.00667	0.00588	0.00515	0.00511	0.00485
0.01807	0.00478	0.00643	0.00560	0.00481	0.00480	0.00459
0.01816	0.00449	0.00619	0.00532	0.00447	0.00449	0.00435
0.01825	0.00420	0.00596	0.00504	0.00413	0.00417	0.00411
0.01833	0.00392	0.00572	0.00475	0.00378	0.00386	0.00389
0.01842	0.00364	0.00548	0.00447	0.00343	0.00355	0.00365
0.01851	0.00338	0.00524	0.00419	0.00308	0.00326	0.00340
0.01860	0.00311	0.00500	0.00391	0.00280	0.00302	0.00315
0.01868	0.00286	0.00476	0.00363	0.00262	0.00279	0.00290
0.01877	0.00261	0.00452	0.00335	0.00244	0.00256	0.00265
0.01886	0.00237	0.00428	0.00306	0.00226	0.00232	0.00240
0.01894	0.00213	0.00404	0.00278	0.00209	0.00209	0.00215
0.01903	0.00190	0.00380	0.00250	0.00191	0.00185	0.00190
0.01912	0.00167	0.00357	0.00228	0.00174	0.00162	0.00165
0.01921	0.00146	0.00333	0.00215	0.00156	0.00139	0.00145
0.01929	0.00124	0.00309	0.00203	0.00139	0.00115	0.00126
0.01938	0.00104	0.00285	0.00191	0.00122	0.00092	0.00107
0.01947	0.00084	0.00261	0.00178	0.00104	0.00072	0.00087
0.01956	0.00064	0.00237	0.00166	0.00087	0.00056	0.00068
0.01964	0.00046	0.00214	0.00154	0.00069	0.00040	0.00049
0.01973	0.00027	0.00190	0.00141	0.00052	0.00024	0.00029
0.01982	0.00010	0.00166	0.00129	0.00035	0.00008	0.00010
0.01990	-0.00007	0.00142	0.00117	0.00017	-0.00008	-0.00009
0.01999	-0.00024	0.00119	0.00104	0.00000	-0.00024	-0.00026
0.02008	-0.00040	0.00101	0.00092	-0.00018	-0.00039	-0.00040
0.02017	-0.00055	0.00099	0.00080	-0.00035	-0.00055	-0.00054
0.02025	-0.00070	0.00097	0.00067	-0.00051	-0.00071	-0.00067
0.02034	-0.00084	0.00095	0.00055	-0.00062	-0.00087	-0.00081
0.02043	-0.00097	0.00093	0.00043	-0.00072	-0.00103	-0.00094
0.02051	-0.00110	0.00091	0.00030	-0.00082	-0.00112	-0.00108
0.02060	-0.00123	0.00089	0.00018	-0.00091	-0.00122	-0.00122
0.02069	-0.00134	0.00087	0.00006	-0.00101	-0.00132	-0.00135
0.02078	-0.00146	0.00084	-0.00006	-0.00111	-0.00142	-0.00149
0.02086	-0.00157	0.00082	-0.00019	-0.00121	-0.00151	-0.00160
0.02095	-0.00167	0.00079	-0.00031	-0.00130	-0.00161	-0.00168
0.02104	-0.00176	0.00075	-0.00043	-0.00139	-0.00171	-0.00176
0.02113	-0.00185	0.00072	-0.00055	-0.00148	-0.00181	-0.00184
0.02121	-0.00194	0.00069	-0.00068	-0.00156	-0.00190	-0.00192
0.02130	-0.00202	0.00066	-0.00080	-0.00165	-0.00200	-0.00199
0.02139	-0.00209	0.00063	-0.00092	-0.00172	-0.00210	-0.00207

Table C-4 (continued)

0.02147	-0.00216	0.00060	-0.00104	-0.00180	-0.00216	-0.00215
0.02156	-0.00223	0.00057	-0.00116	-0.00188	-0.00220	-0.00223
0.02165	-0.00228	0.00054	-0.00131	-0.00195	-0.00224	-0.00231
0.02174	-0.00234	0.00051	-0.00129	-0.00202	-0.00228	-0.00237
0.02182	-0.00239	0.00049	-0.00126	-0.00209	-0.00232	-0.00239
0.02191	-0.00243	0.00046	-0.00123	-0.00216	-0.00236	-0.00242
0.02200	-0.00246	0.00043	-0.00120	-0.00222	-0.00240	-0.00244
0.02209	-0.00250	0.00041	-0.00117	-0.00228	-0.00243	-0.00247
0.02217	-0.00252	0.00038	-0.00114	-0.00231	-0.00247	-0.00249
0.02226	-0.00254	0.00036	-0.00111	-0.00230	-0.00251	-0.00252
0.02235	-0.00256	0.00034	-0.00108	-0.00229	-0.00255	-0.00254
0.02243	-0.00257	0.00032	-0.00105	-0.00228	-0.00257	-0.00256
0.02252	-0.00258	0.00029	-0.00103	-0.00226	-0.00255	-0.00259
0.02261	-0.00258	0.00027	-0.00100	-0.00225	-0.00254	-0.00261
0.02270	-0.00257	0.00025	-0.00097	-0.00224	-0.00252	-0.00258
0.02278	-0.00256	0.00023	-0.00094	-0.00223	-0.00250	-0.00256
0.02287	-0.00255	0.00022	-0.00091	-0.00221	-0.00248	-0.00253
0.02296	-0.00253	0.00020	-0.00088	-0.00220	-0.00246	-0.00250
0.02304	-0.00251	0.00018	-0.00085	-0.00218	-0.00244	-0.00247
0.02313	-0.00248	0.00017	-0.00082	-0.00217	-0.00242	-0.00244
0.02322	-0.00244	0.00015	-0.00079	-0.00216	-0.00240	-0.00241
0.02331	-0.00240	0.00014	-0.00076	-0.00214	-0.00238	-0.00238
0.02339	-0.00236	0.00012	-0.00073	-0.00213	-0.00236	-0.00235
0.02348	-0.00231	0.00011	-0.00070	-0.00211	-0.00229	-0.00232
0.02357	-0.00225	0.00010	-0.00067	-0.00210	-0.00221	-0.00227
0.02366	-0.00219	0.00008	-0.00064	-0.00208	-0.00214	-0.00219
0.02374	-0.00213	0.00007	-0.00061	-0.00197	-0.00206	-0.00211
0.02383	-0.00206	0.00006	-0.00058	-0.00187	-0.00199	-0.00203
0.02392	-0.00199	0.00005	-0.00055	-0.00176	-0.00191	-0.00194
0.02400	-0.00191	0.00004	-0.00052	-0.00166	-0.00184	-0.00186
0.02409	-0.00182	0.00004	-0.00049	-0.00156	-0.00176	-0.00178
0.02418	-0.00173	0.00003	-0.00045	-0.00145	-0.00169	-0.00170
0.02427	-0.00164	0.00002	-0.00042	-0.00135	-0.00161	-0.00162
0.02435	-0.00154	0.00002	-0.00039	-0.00124	-0.00154	-0.00153
0.02444	-0.00144	0.00001	-0.00036	-0.00114	-0.00143	-0.00145
0.02453	-0.00133	0.00001	-0.00032	-0.00103	-0.00130	-0.00133
0.02461	-0.00122	0.00000	-0.00029	-0.00093	-0.00117	-0.00120
0.02470	-0.00110	0.00000	-0.00026	-0.00082	-0.00104	-0.00107
0.02479	-0.00098	0.00000	-0.00023	-0.00072	-0.00091	-0.00093
0.02488	-0.00086	0.00000	-0.00019	-0.00061	-0.00078	-0.00080

Table C-4 (continued)

0.02496	-0.00072	0.00000	-0.00016	-0.00051	-0.00065	-0.00066
0.02505	-0.00059	0.00000	-0.00012	-0.00040	-0.00052	-0.00053
0.02514	-0.00045	0.00000	-0.00009	-0.00030	-0.00039	-0.00040
0.02523	-0.00030	0.00000	-0.00006	-0.00019	-0.00026	-0.00026
0.02531	-0.00015	0.00000	-0.00002	-0.00009	-0.00013	-0.00013
0.02540	0.00000	0.00000	0.00000	0.00000	0.00000	0.00000

APPENDIX D

SENSITIVITY ANALYSES RESULTS

Effects of various drilling parameters on surge and swab pressure gradient are presented in charts and discussed in Chapter 4 and Chapter 5 of this study. The sensitivity analyses results are numerically tabulated in this Appendix.

Table D-1, Table D-2, and Table D-3 show effect of different parameters on surge and swab pressure gradient using Newtonian fluids.

Table D-1. Inputs and Outputs of Effect of Viscosity on Surge and Swab Pressure Gradients with Different Pipe Velocities

Diameter Ratio	0.653	0.653	0.653	0.653	0.653
Viscosity (Pa.s)	0.1	0.3	0.5	0.7	0.9
Pressure Gradient @ Vp=0.1 m/s (kPa/m)	0.013	0.038	0.063	0.088	0.114
Pressure Gradient @ Vp=0.4 m/s (kPa/m)	0.051	0.152	0.253	0.354	0.455
Pressure Gradient @ Vp=0.7 m/s (kPa/m)	0.088	0.265	0.442	0.619	0.796
Pressure Gradient @ Vp=1.0 m/s (kPa/m)	0.126	0.379	0.631	0.884	1.137
Pressure Gradient @ Vp=1.3 m/s (kPa/m)	0.164	0.492	0.821	1.149	1.477

Table D-2. Inputs and Outputs of Effect of Pipe Velocity on Surge and Swab Pressure Gradients with Different Diameter Ratios

Viscosity (Pa.s)	0.9	0.9	0.9	0.9	0.9
Pipe Velocity (m/s)	0.1	0.2	0.3	0.4	0.5
Pressure Gradient @ Ri/Ro=0.65306 (kPa/m)	0.114	0.227	0.341	0.455	0.568
Pressure Gradient @ Ri/Ro=0.700 (kPa/m)	0.180	0.361	0.541	0.721	0.901
Pressure Gradient @ Ri/Ro=0.750 (kPa/m)	0.321	0.641	0.962	1.282	1.603
Pressure Gradient @ Ri/Ro=0.800 (kPa/m)	0.641	1.283	1.924	2.565	3.207
Pressure Gradient @ Ri/Ro=0.850 (kPa/m)	1.564	3.129	4.693	6.258	7.822

Table D-3. Inputs and Outputs of Effect of Diameter Ratio on Surge and Swab Pressure Gradients with Different Viscosities

Pipe Velocity (m/s)	0.1	0.1	0.1	0.1	0.1
Diameter Ratio	0.203	0.218	0.233	0.249	0.265
Pressure Gradient @ μ=0.1 Pa.s (kPa/m)	0.013	0.020	0.036	0.071	0.174
Pressure Gradient @ μ=0.3 Pa.s (kPa/m)	0.038	0.060	0.107	0.214	0.521
Pressure Gradient @ μ=0.5 Pa.s (kPa/m)	0.063	0.100	0.178	0.356	0.869
Pressure Gradient @ μ=0.7 Pa.s (kPa/m)	0.088	0.140	0.249	0.499	1.217
Pressure Gradient @ μ=0.9 Pa.s (kPa/m)	0.114	0.180	0.321	0.641	1.564

Effect of various drilling parameters on surge and swab pressure gradient for YPL fluids are presented in below Table D-4, Table D-5, Table D-6, and Table D-7.

Table D-4. Inputs and Outputs of Effect of Pipe Velocity on Surge and Swab Pressure Gradients with Different Flow Behavior Indices

Yield Stress (Pa)	2	2	2	2	2
Diameter Ratio	0.65	0.65	0.65	0.65	0.65
Consistency Index (Pa.s)	0.5	0.5	0.5	0.5	0.5
Pipe Velocity (m/s)	0.1	0.3	0.5	0.7	0.9
Pressure Gradient @ n=0.5 (Pa/m)	67.275	88.408	102.709	114.269	124.243
Pressure Gradient @ n=0.6 (Pa/m)	74.213	105.223	127.854	146.952	163.935
Pressure Gradient @ n=0.7 (Pa/m)	82.098	126.726	161.931	192.954	221.382
Pressure Gradient @ n=0.8 (Pa/m)	91.028	154.374	208.392	258.078	304.962
Pressure Gradient @ n=0.9 (Pa/m)	101.179	190.158	272.114	350.707	427.078

Table D-5. Inputs and Outputs of Effect of Yield Stress on Surge and Swab Pressure Gradients with Different Pipe Velocities

Diameter Ratio	0.65	0.65	0.65	0.65	0.65
Consistency Index (Pa.s)	0.5	0.5	0.5	0.5	0.5
Flow Behavior Index	0.5	0.5	0.5	0.5	0.5
Yield Stress (Pa)	2	4	6	8	9
Pressure Gradient @ Vp=0.1 m/s (Pa/m)	67.275	107.528	147.929	188.478	208.720
Pressure Gradient @ Vp=0.3 m/s (Pa/m)	88.408	130.327	171.857	213.448	234.274
Pressure Gradient @ Vp=0.5 m/s (Pa/m)	102.709	145.634	187.983	230.226	251.361
Pressure Gradient @ Vp=0.7 m/s (Pa/m)	114.269	157.886	200.855	243.620	264.996
Pressure Gradient @ Vp=0.9 m/s (Pa/m)	124.243	168.384	211.845	255.047	276.622

Table D-6. Inputs and Outputs of Effect of Flow Behavior Index on Surge and Swab Pressure Gradients with Different Diameter Ratios

Yield Stress (Pa)	2	2	2	2	2
Pipe Velocity (m/s)	0.1	0.1	0.1	0.1	0.1
Consistency Index (Pa.s)	0.5	0.5	0.5	0.5	0.5
Flow Behavior Index	0.5	0.6	0.7	0.8	0.9
Pressure Gradient @ Ri/Ro=0.65 (Pa/m)	67.275	74.213	82.098	91.028	101.179
Pressure Gradient @ Ri/Ro=0.68 (Pa/m)	76.938	85.888	96.236	108.192	122.074
Pressure Gradient @ Ri/Ro=0.71 (Pa/m)	89.285	101.069	114.970	131.408	150.966
Pressure Gradient @ Ri/Ro=0.74 (Pa/m)	105.706	121.668	140.967	164.402	193.057
Pressure Gradient @ Ri/Ro=0.77 (Pa/m)	127.841	150.099	177.787	212.425	256.075

Table D-7. Inputs and Outputs of Diameter Ratio on Surge and Swab Pressure Gradients with Different Yield Stresses

Pipe Velocity (m/s)	0.1	0.1	0.1	0.1	0.1
Consistency Index (Pa.s)	0.5	0.5	0.5	0.5	0.5
Flow Behavior Index	0.5	0.5	0.5	0.5	0.5
Diameter Ratio	0.65	0.68	0.71	0.74	0.77
Pressure Gradient @ τ_0=2 Pa (Pa/m)	67.275	76.938	89.285	105.706	127.841
Pressure Gradient @ τ_0=4 Pa (Pa/m)	107.528	121.134	138.297	160.787	190.605
Pressure Gradient @ τ_0=6 Pa (Pa/m)	147.929	165.420	187.243	215.600	252.778
Pressure Gradient @ τ_0=8 Pa (Pa/m)	188.478	209.849	236.381	270.617	315.096
Pressure Gradient @ τ_0=9 Pa (Pa/m)	208.720	232.116	261.002	298.147	346.363